Reply to referees #1 and 2 on "Lidar profiling of aerosol optical properties from Paris to Lake Baikal (Siberia)" by E. Dieudonné et al.

We would like to thank the two anonymous referees for their constructive comments that helped us a lot to improve this paper. In this document, our replies to the referees' comments are followed by the revised manuscript, with corrections highlighted in blue. At the very end is a study of the errors on PDR in response to the referees' main concerns.

I. General comments

1.1 BER or LR

Referee #1: *I strongly recommend to switch from BER (backscatter to extinction ratio) to LIDAR RATIO (extinction-to-backscatter ratio)… in general! From the literature it becomes obvious that nobody uses BER except lidar groups in France. So please move to the international standard in this point.*

Referee #2: *I also recommend to use the extinction-to-backscatter ratio (LR) than BER, because it is more standard. If you feel to need to use the BER in radiation discussions elsewhere, then you can inverse it.*

Both referees strongly suggested switching from the backscatter-to-extinction ratio (BER) to the more commonly used extinction-to-backscatter ratio (so called lidar ratio or LR). Although we tried to give the equivalent LR values in our discussion paper, we understand that readers accustomed to working with LR would feel annoyed to convert from BER to LR. Therefore, we bow to the majority and present a revised paper using LR instead of BER. Please note, however, that BER has a more physical meaning because it explains the probability to backscatter a photon. Possible differences between the discussion and revised paper can arise from the fact that the average of the inverse is of course different from the inverse of the average...

1.2 High values of lidar ratio

Referee #1: *Average BER is 0.017 ± 0.009 sr^{-1} means you found an average lidar ratio = 58.8 sr with a standard deviation from 38.5 to 125 sr. I am surprised because the lidar ratio is the more direct parameter in the Fernald retrieval and should show a well-known symmetric behavior around the mean value, i.e. from 38 to 78 sr. I conclude that the error in*

all the found results is rapidly increasing if the BER values are below 0.012 which is already an unrealistically low number to my opinion. Even in polluted China it is hard to observe any lidar ratio above 80sr (or BER = 0.0125 sr^{-1}).

Section 3.3. All the BER or lidar ratio numbers, you present, are simply dangerous. Lidar ratio values of 171 sr!!! Who shall believe that? As already mentioned it is hard to find lidar ratios above 80sr in the literature. Even in such high aerosol pollution cases, the aerosol particles must be rather small and highly absorbing. And now you come with values even a factor of 2 higher…, at conditions with omnipresent road dust (coarse particles), always mixed upward in the convective boundary layer. And then you state: mean value is 58 sr with a standard deviation of 41 sr. How is it possible to observed particle lidar ratios down to 20, 10 or even 0 sr…, over a polluted dusty continent, far away from any marine particle sources…? So, all this is simply not convincing, not trustworthy.

Figure 10 (Kazan case study). All values below 1500m are rather questionable. Below 1500 m, all lidar ratios are between 100 and 200 sr or even higher. This is unrealistic... and puts a question mark to all values of the tour for heights below 1500 m.

Referee #2: *The LR values indicated here are rather higher than the literature even dust and smoke.*

Following the suggestion by referee #1, we checked the shape of the LR distribution provided by the Monte-Carlo algorithm associated with the constrained Klett inversion on the 300-700 m a.g.l. layer ("systematic treatment" used in Section 3). This distribution is indeed Gaussian for a majority of cases, yet there are outliers which are due to a bad convergence of the inversion algorithm on cases with unsufficient aerosols load. This conducted us to reject those profiles that were previously included in the BER histogram (Fig. 6) and in the PDR vs LR scatter plot (Fig. 7) (we removed the profiles for which the LR distribution was not Gaussian or only partly converged). This greatly reduced the scattering towards unrealistically high LR values (see Fig. 3 in the revised paper).

Also in the case studies (multi-layer constrained Klett inversion), the layers were the LR appears as 10 or 130 sr are in fact layers were convergence could not be reached, most often because the aerosol load is too low to provide a good constraint. We have now removed those values in the profiles.

Apart from these rejected profiles, it is true that several LR values fall in the upper range of what is reported in the literature. However, values of 90 sr at 355 nm have been observed in Paris (e.g. Raut and Chazette, 2009; Royer et al., 2011, N_2-Raman lidar) or in the Po Valley (Royer et al., 2010, CALIOP/MODIS synergy).

1.3 Overlap function

Referee #1: *Are you sure that there is no overlap effect for the lowest 700 m of the atmosphere in your Raman lidar solutions so that the extinction values are overestimated or underestimated, when you correct for overlap effects. You have to correct for overlap effects, for sure! Do you know the overlap function?*

Yes, we do know the overlap function. It was measured before the trip and verified along the route under fair weather afternoon cumulus clouds at different points of the journey, and complete overlap is around 250 m. A paragraph was added about that after the instrument description.

1.4 Photomultiplier detection mode

Referee #2: *I have a strong doubt in this mini Raman/polarization lidar instrumentation at 355 nm, because they use only the analog detection (Royer et al, 2011) though that a large dynamic range is more necessary in UV-lidar signals. Simultaneous photon counting is indispensable for retrieval of the lidar ratio (LR) and the particle depolarization ratio (PDR) possible at nighttime and maybe the results can be extent to the daytime data. This fact deteriorate to convince the observed important optical parameters, LR, PDR of aerosols for public.*

The signals were recorded both in the analog and photon-counting detection mode and merged for optimal SNR. This is an important difference with the reference we give for our instrument (Royer et al., 2011); we should indeed have mentioned that and Section 2.2 has been completed about this point. Note that counting mode cannot be used during daytime.

1.5 Error on the Particle Depolarization Ratio (PDR)

One of the main concern of referee #1, which is also mentioned by referee #2, is the reliability of our PDR measurements.

Referee #1: *Regarding the depolarization ratios presented: Volume depolarization ratios at 355 nm can be well measured even if the laser light always contains a few percent of depolarized radiation. Usually only 98 % of the transmitted laser light is fully linearly polarized. One can see this if one looks at the 355 nm volume depolarization ratio in the Rayleigh atmosphere. Here the volume depolarization ratio is typically 2 % and not 0.7 % as the theory tells you for an ideal polarization lidar receiver unit. Now, taken this source of uncertainty into account how can you then measure volume depolarization ratios below 2% and obtain even particle depolarization ratios close to 1 %. This is simply impossible. Furthermore, the uncertainty in the retrieved particle depolarization ratio is especially high at 355 nm (compared to 532 and 1064 nm). Please provide uncertainty information and may be show a figure with the profile of the volume depolarization ratio, and the related particle depolarization ratio together with the particle backscatter coefficient profile to convince the reader. […]*

The depolarization ratios are clearly of low quality. You obviously were not able to perform ±45° measurements from time to time during the trip in order to check, day by day, the polarization lidar performance. This is critical in case of moving platforms (making measurements at dirty roads) with strongly varying temperature and humidity conditions in the receiver unit. How I shall accept that all your polarization measurements are of high quality? Furthermore, as already mentioned above, the determination of the PDR at 355 nm is most critical. Experience shows that a proper 355nm PDR measurement is only possible

down to low particle backscatter coefficients when they reach the Rayleigh backscatter values, so for backscatter ratios around 2, at least 1.5, but by no means down to values as low as 1.005. How did you came to this conclusion (1.005)? This is a so unrealistically low value!

Regarding proper 355 nm polarization lidar measurements, please have a look into the SAMUM paper of Freudenthaler et al. (2009). Freudenthaler has the highest experience with polarization lidars. His lidars in Munich have the highest quality standard possible. But for 355 nm, the PDR values of the Munich lidars have typical uncertainties of 20-50%! Even within pronounced dust layers close to the Sahara! So please come up with a realistic view on the quality of your PDR observations, and afterwards, just show the most reliable values (in mixed dust and pure dust layers)… please come up with realistic uncertainties and a realistic range of backscatter ratios for which the PDR values of your lidar are roughly trustworthy.

Referee #2: *The error of the PDR is large when the aerosol loading is small. And as pointed out by the referee #1, the error is strongly depend on the matching (boundary) condition at Rayleigh scattering dominant high altitudes and the gain ratio. The value close to 1 % seems meaningless and embedded in the errors.*

Referee #1 states that regular measurements at ±45° are necessary in order to properly calibrate the gain ratio between the parallel (total in our case) and perpendicular polarization channels of the lidar. We think that this is indeed necessary at 1064 and 532 nm, but not at 355 nm: as the molecular signal is much stronger at this wavelength, it can be used to directly calibrate the gain ratio by normalizing the volumetric depolarization ratio (VDR) to its molecular value (0.39% given our filter bandwidth of 0.2 nm). To take into account cross-talk between channels, the separating plates were precisely characterized before the experiment as in Chazette et al. (2012). Of course, if residual aerosols are present in the supposedly molecular layer used for calibration, it can cause errors on the gain ratio retrieval. However, we have one full night of observations near Baikal Lake with a completely clean free troposphere that provided us with a reliable gain ratio value.

Referee #1 also states that gain ratio calibration is particularly critical for moving platforms, probably referring to the sensitivity of the polarization separation to mechanical stability. In our instrument, we use an "X squared" High Extinction Polarizer plate instead of a Brewster plate as its reflectance/transmittance coefficients are less sensitive to a change in the incident angle. Also, similar values of the gain ratio (deviating by no more than 5 % from the aforementioned reference value obtained at Baikal) were obtained on other clean nights above Riga (Latvia) and Pskov (just after the Russian border), so that we have good reasons to think that our gain ratio was stable along the journey. This 5% uncertainty is taken into account in the PDR error.

Referee #1 also states that PDR measurements are possible at 355 nm only under very large aerosol loads, corresponding to scattering ratio values (total to molecular backscatter ratio or SR) higher than 1.5 or even 2. We disagree on this point: a simulation of our instrument shows that in the noise conditions between Kazan to Nizhny-Novgorod, the scattering ratio threshold for reliable PDR measurements (<10% relative error) is below 1.02. We present the full results of this error simulation specifically for the reviewers in an attached PDF file. A demonstration has been added

in Appendix B of the revised paper. In the paper, we now discard PDR retrievals for scattering ratios below 1.05. A shorter paragraph about error calculation has been added to the section regarding PDR retrieval (Sec. 2.3, now 2.4). For the systematic processing (retrieval of the LR and PDR in the 300-700 m a.gl. layer), the uncertainty is estimated *(i)* by varying the channels gain ratio and plate coefficients by ±5 %, *(ii)* by varying the lidar ratio by ±10 sr and *(iii)* through the standard deviation of the PDR in the layer (atmospheric variability); the 3 sources are then combined through a quadratic sum. This uncertainty was used to add error bars on Figures 5 and 7 (pp. 27932 &27934, now Fig. 3 and 4).

1.6 Length of the text

Referee #1: *Length and boring description… Please try to present a compact text, the shorter the better! […] I stopped to read all this…, the text is simply too long, nobody is really interested in all these details. […]Very long and exhausting, please shorten, provide the most interesting numbers and facts.*

Referee #2: *Certainly shorten and high lighten the paper for ACP readers.*

The whole paper has been peered through to shorten the text and stick to the essential information.

1.7 Figures

Referee #1: *The journey with the lidar is a unique story. Besides the requirement to check and discuss all the results and numbers carefully, an important point is to improve the figures significantly. At the moment, the figures are partly rather small, not readable, or simply of low quality… […]The figures are not in a good shape and need to be improved significantly to properly illustrate this unique trip.*

Maps and several figures have been improved. The small size of some of the figures is mainly due to the landscape format on A5 paper of ACPD. The portrait format on A4 paper of ACP will allow enlarging these figures substantially, thus improving readability.

II. Detailed comments

1.8 Comments common to both referees

Figure 1 (p. 27928): itinerary map.

Referee #1: *Why not starting with a simple well-illustrated map, showing the route, the different countries, the different sites for your longer measurements, and the orography: mountains, may be desert areas etc. In this way the reader would become easily familiar with all detailed geographical information along the unique route of the journey.*

Referee #2: *Figures 1, 4, I also want to see the geographical view the Europe and Russia. I have to often look into my map book to check the levels and desert area and so no.*

Both referees asked for this figure to give more geographical information (country names, location of the main desert areas etc.). Therefore, we replaced the EDGAR PM_{10} emissions used as background of the map (Fig. 1) by a MODIS true color reflectance image similar to what is used on Google Earth for instance. This makes the forest or desert areas directly visible on the map plus we added labels for the main cities along the trip, some of the countries, mountains, lakes, seas and desert areas. Referee #1 also requested some information about the population density, so we considered adding dots with a size representing the number of inhabitants but this would have made the map unreadable.

About the dusty mix case study in Ishim (p. 27914).

Referee #1: *A mean BER of 0.011 sr^{-1} (lidar ratio of 90 sr) for a mixture of dust and smoke…? I do not believe!*

Referee #2: *Since the specific observation results the dusty-mix case is not shown at all (only the values Table 1), the dusty-mix case study can be omitted. ACP readers expect clear evidences in this vast area not explored by the ground-based lidar frequently and typical aerosol events.*

This dusty-mix case corresponds to a thin layer. Therefore, considering the vertical averaging introduce by the Gaussian derivative filter, it is possible that the retrieved LR in the dust layer is contaminated by the PBL (located just below) of the biomass burning layer (located above). Moreover, this dust layer was observed around sunset, i.e. not in optimal SNR conditions so that a wide filter width was required. For those two reasons, we removed this dusty mix case from the paper. The Ishim case was maintained for biomass burning as the smoke layer does not suffer from the same problems as the dust layer. For dusty-mix cases, the Kazan observations already provide a value so we based on this case instead.

1.9 Comments from referee #1

Introduction (pp. 27882-27885). *12 Mhab is slang…, please improve.*

The abbreviation Mhab was replaced by million inhabitants. Regarding references, see our comment "bibliography" below.

Section 2.1 (pp. 27885-27886): itinerary.

Did you check the web page of the Leipzig lidar group for potential comparison? To my knowledge they conduct continuous lidar monitoring with a Raman lidar there. Could be used for comparison, may be to check the BER values and particle depolarization ratios.

Unfortunately, there are no observations for the day we passed near Leipzig (June 6th 2013), nor for the previous or following day. A sentence was added about that in Section 3.4 (now 3.3) of the paper (comparison to MODIS & AERONET).

Section 2.2 (pp. 27887-27892) and Figures 2 and 3 (pp. 20929-20930): LR and extinction retrieval.

Do we really need to start with the basic lidar equation? A clear NO… from my side. Readers of ACP expect atmospheric results. All your theoretical framework is certainly well described elsewhere. So, please provide proper reference and keep all the methodology sections as short as possible. Note, only if papers are short, compact, and highlight the main findings only, many people will read them.

Referee #1 states there is no need to start back from the lidar equations and detail so much the retrieval process in ACP. We therefore shortened this section a lot (and removed the related figures) in order to present only the main steps of the data processing. A few details are now given in Appendix A.

Section 3.2 (p. 27896).

PDR dust values at 355 nm are typically 25% or less (see SAMUM papers of Freudenthaler et al., 2009 and Groß et al., 2011). Your dust 355 nm PDR value of 37% for desert dust is clearly too high.

Please keep in mind that this PDR value was derived using the campaign average LR in the boundary layer, and not using an optimized LR for desert dust particles, which makes the uncertainties large. Besides, the point of this section is to discuss the general distribution of aerosols in Russia, based on a systematic processing; the precise determination of dust optical properties of is based on the case studies presented in Section 4. Please note, however, that PDR values of 38 ± 4 % have been retrieved at 355 nm, though it was in a volcanic ash layer (Ansmann et al., 2011). A sentence was added about all that in the paper.

Bibliography (pp. 27919-27924) and tables 1-3 (pp. 27925-27927).

Please use the latest paper of Pappalardo et al. (2014, EARLINET special issue introductory paper) as a reference for EARLINET. […] The appropriate reference for INDOEX is Ramanathan et al. (2001) introductory paper to INDOEX. […]We need an improved aerosol-related reference for the ZOTTO tower, e.g. Heintzenberg et al. (2011).

Better references to 355 nm PDR: Freudenthaler et al. (2009) and Groß et al. (2011)

Besides Cattrall et al. (2005) there is now a much better AERONET paper on desert dust lidar ratios available: Schuster et al. (2012). For Arabian dust lidar ratios, please have look into Mamouri et al. (2013) too. […]There are many lidar ratio papers over the Mediterranean (EARLINET) for dust: Amiridis et al. (2005), Mona et al. (2006), Papayannis et al. (2008), and references therein…

Please check the papers of Franke et al. (2001, 2003) for lidar ratios over the Indian Ocean during INDOEX… […] Mattis et al. (2004) summarized 355 nm lidar ratios for Leipzig (EARLINET period from 2000-2003), please have a look!

There is a new paper of Nisantzi et al. (2014). The authors discuss the possibility of soil dust injection into the atmosphere during biomass burning events. This option may hold even here, for Russia.

The references for the EARLINET lidar network, for the INDOEX and SAMUM field campaigns, and for the ZOTTO tower have been changed following the recommendations by referee #1. Tables 1 and 2 have been updated to include the papers from Schuster et al. (2012), Mamouri et al. (2013) and Amiridis et al. (2005, 2009) as suggested by referee #1 but the literature is simply too vast to mention all papers about dust. Some of the references also suggested by referee #1 (e.g. Mattis et al., 2004) were not included originally because the values were reused in the paper by Müller et al. (2007). As the latter belongs to the same research group, we felt that mentioning only the overview paper was sufficient; however, the original references have now been added to the 3 Tables. The reference to Nisantzi et al. (2014) has been added to the discussion about dust lifting by fires.

Pure dust PDR values of 16-20% are simply wrong (at least misleading), these authors (Chazette et al., 2014) obviously measured mixtures of dust with smoke, urban haze and/or marine particles…

This reference was moved in the dusty-mix section.

Figures 4 and 5 (pp. 27931-27932): aerosol optical thickness (AOT) map and AOT-PDR frieze.

Figure 4: Again, everything is so small, please enlarge the symbols. However, may be show the map as top plot, and below (bottom plot) show a bar chart for the optical depth, the length shows the AOT value. This is better than color coded small circles. Or use the layout for AOT as in Figure 4, at least color coded is not of advantage here.

Figure 5: Again, all the symbols are too small, you may better use clearly different symbols for PBL and FT, may be circles and crosses (or stars). Detailed information on PDR below 3% is useless… What about linear scale?

Both figures have been merged following suggestion by referee #1 to use stacked bar charts for the AOT. As discussed in the General comments, there is a meaning in the small values of PDR so we want to be able to distinguish a 1 % and a 3 %, which would be impossible in linear scale given the maximum values.

Figure 7 (p. 27934).

This figure is to my opinion useless, keeping the large uncertainty in all PDR values in mind, and here you show the range up to PDR = 6% only… I do not see a clear message!

Error bars have been added to this figure, using the uncertainties evaluated following the method described in the general comment section. The PDR range is limited to 6 % because this figure shows LR and PDR values between 300 and 700 m a.g.l., not in the elevated dust layers, and because only the convergent profiles are included. The profiles for which desert dust was mixed from the free troposphere into the boundary layer are not convergent, and they are the only ones for which a strong depolarization in the lower PBL was observed.

Figure 9 (p. 27936). It was removed as requested by referee #1.

Figures 11-12 (pp. 27938-27939), and 15-16 (pp. 27942-27943): AOT & extinction, PDR quicklooks.

Figure 11 and 12 should be shown together (top plot and bottom plot).

Following suggestion by referee #1, these figures have been merged as top, middle and bottom plot.

Figures 13 and 17 (pp. 27940 & 27944): HYSPLIT back-trajectories.

These trajectory plots are not helpful. The information content is close to zero for readers. Why not simplify the message? Just show a few representative trajectories including height information as in these typical HYSPLIT plots and then indicate the desert areas, too. You do not have to demonstrate that you are a critical user and expert of trajectories. Please provide a clear message! This is the most important task!

When running the model in the standard mode, we ended up with back-trajectories that stayed in the free troposphere for 7 days or did not go to desert areas (trajectories in bold line on the figures). However, we did observed dust… so we had to assume this was due to trajectory errors, which can be significant on such a long period. Because we are no HYSPLIT experts, we used the ensemble mode that is precisely designed to assess trajectory errors instead of manually varying the ending point or time until finding a trajectory that suited us. Then, we could have plotted only a few selected trajectories among the 27, but on which basis to choose? Besides, the idea was to show the dispersion as after 7 days, since an air mass does not have one single well-defined origin.

1.10 Comments from referee #2

Choice of the itinerary.

Why the route is almost along with 55 degree north in latitude? Convenience or scientific interest?

The itinerary was chosen so as to limit potential problems at the customs. We wanted to directly enter Russia from the European Union instead of crossing Belarus or Ukraine, which directed us to the Baltic countries. For the same reason, we preferred not to enter

Kazakhstan so it was not possible to travel more to the south. Driving more to the north was not possible either, because there is only one trans-Siberian road after Chelyabinsk. Nevertheless, many undocumented interesting hot spots are visited using this road.

Figures 11-12 (pp. 27938-27939), and 15-16 (pp. 27942-27943): AOT & extinction, PDR quicklooks.

Backscattering coefficient or scattering ratio than extinction coefficient and recommended in Figures 11 and 15 because the extinction coefficient is rather sensitive to the LR in the Klett inversion.

Following the suggestion by referee #2, we plotted the particle backscatter coefficient instead of the extinction, as it is indeed less sensitive to the error on the lidar ratio. Referee #2 also points that the z-axis range is not the same for extinction (now backscatter) and PDR; this is because the maximum range for accurate PDR is limited by the sky background, so there is no point in plotting it up to the same altitude. To make comparison easier, we used the same aspect ratio for altitude on both figures but this aspect was lost when the figures were integrated into the PDF document. However, now that Figures 11-12 and 15-16 have been merged, the aspect ratio will be conserved.

III. Main changes in the manuscript

General: all results are now presented in terms of lidar ratio instead of BER.

Section 2.1 (now 2.2): instrument characteristics. A precision about the acquisition mode (photon-counting) was added, as long as a paragraph about the overlap determination.

Section 2.2 (now 2.3): LR & extinction retrieval. This section was shortened a lot and some information was moved to Appendix A.

Section 2.3 (now 2.4): PDR retrieval. Precisions on the error calculation have been added here and in Appendix B.

Section 3.1: retrieval process for the systematic analysis. This section was removed now that Section 2.3 summarizes better the processing applied to the data.

Section 3.3: classification of boundary layer aerosols. The BER (now LR) distribution has been moved to a new Section 3.1 so that Section 3 starts in a more logical way, by explaining the choice of the lidar ratio used in the rest of this systematic treatment.

Sections 3.2 and 3.3: these two sections have been merged so that Figure 5 (now Fig. 3, map of the lidar AOT and PDR along the journey) and Figure 7 (now Fig. 4, boundary layer PDR vs LR scatter plot) can be discussed together. This allows to reduce the repetitions in the text.

Sections 3.4 (now 3.3) and 4: The text was shortened (particularly to remove unnecessary details about the lidar retrieval or soil geology in Sec. 4).

Section 4: the plan was changed to group the discussion about back-trajectories in a single subsection. It is now:

4.1. Case studies
4.1.1. Dust and biomass burning aerosols observed west of Kazan
4.1.2. Dust and biomass burning aerosols observed above Omsk
4.2. Origin of the elevated layers
4.3. Discussion
4.3.1. Desert dust
4.3.2. Biomass burring aerosols

Appendices: additional information about the retrieval has been moved to Appendix A and a study about the PDR uncertainties has been added in Appendix B.

Figure 1: the background of the itinerary map is now a satellite image (MODIS true color reflectance) instead of a PM_{10} emission map.

Figures 2 and 3 have been removed.

Figure 4 and 5 (now Fig. 3) have been merged. Error bars have been added on the PDR values.

Figure 6 (now Fig. 2): profiles for which only part of the Monte-Carlo distribution converged to a LR value have been removed from the LR distribution. Now that only best quality data are included in the LR distribution, it is much less scattered towards unrealistically high LR values.

Figure 7 (now Fig. 4): error bars have been added on the LR and PDR values.

Figure 10 (now Fig. 6): the left panels now displays the particle backscatter instead of the extinction, plus the scattering ratio. A right panel displaying the Volumetric Depolarization ratio and PDR has been added to show the intermediates of the PDR retrieval.

Figures 11 & 12 (now Fig. 7): these figures have been merged. The particle backscatter is shown instead of the extinction. The same changes were made for Figures 15 & 16 (now Fig. 9).

Figures 13 & 17 (now Fig. 10 & 11): the background of the map is now a satellite image (MODIS true color reflectance). Geographical indications have been added (country, mountains or sea names) and MODIS fire hotspots are directly plotted on the map.

IV. References

Amiridis, V., Balis, D. S., Giannakaki, E., Stohl, A., Kazadzis, S., Koukouli, M. E. and Zanis, P.: Optical characteristics of biomass burning aerosols over Southeastern Europe determined from UV-Raman lidar measurements, Atmos. Chem. Phys., 9(7), 2431–2440, doi:10.5194/acp-9-2431-2009, 2009.

Amiridis, V., Balis, D. S., Kazadzis, S., Bais, A., Giannakaki, E., Papayannis, A. and Zerefos, C.: Four-year aerosol observations with a Raman lidar at Thessaloniki, Greece, in the framework of European Aerosol Research Lidar Network (EARLINET), J. Geophys. Res., 110, D21203, doi:10.1029/2005JD006190, 2005.

Ansmann, A., Tesche, M., Seifert, P., Groß, S., Freudenthaler, V., Apituley, A., Wilson, K. M., Serikov, I., Linné, H., Heinold, B., Hiebsch, A., Schnell, F., Schmidt, J., Mattis, I., Wandinger, U. and Wiegner, M.: Ash and fine-mode particle mass profiles from EARLINET-AERONET observations over central Europe after the eruptions of the Eyjafjallajökull volcano in 2010, J. Geophys. Res. Atmos., 116, doi:10.1029/2010JD015567, 2011.

Cattrall, C., Reagan, J., Thome, K. and Dubovik, O.: Variability of aerosol and spectral lidar and backscatter and extinction ratios of key aerosol types derived from selected Aerosol Robotic Network locations, J. Geophys. Res., 110, D10S11, doi:10.1029/2004JD005124, 2005.

Chazette, P., Dabas, A., Sanak, J., Lardier, M. and Royer, P.: French airborne lidar measurements for Eyjafjallajökull ash plume survey, Atmos. Chem. Phys., 12(15), 7059–7072, doi:10.5194/acp-12-7059-2012, 2012.

Chazette, P., Marnas, F. and Totems, J.: The mobile Water vapor Aerosol Raman LIdar and its implication in the framework of the HyMeX and ChArMEx programs: application to a dust transport process, Atm. Meas. Tech., 7(6), 1629–1647, doi:10.5194/amt-7-1629-2014, 2014.

Franke, K., Ansmann, A., Müller, D., Althausen, A., Wagner, F. and Scheele, R.: One-year observations of particle lidar ratio over the tropical Indian Ocean with Raman lidar, Geophys. Res. Lett., 28(24), 4559–4562, doi:10.1029/2001GL013671, 2001.

Franke, K., Ansmann, A., Müller, D., Althausen, D., Venkataraman, C., Shekar Reddy, M., Wagner, F. and Scheele, R.: Optical properties of the Indo-Asian haze layer over the tropical Indian Ocean, J. Geophys. Res., 108(D2), 4059, doi:10.109/2002JD002473, 2003.

Freudenthaler, V., Esselborn, M., Wiegner, M., Heese, B., Tesche, M., Ansmann, A., Müller, D., Althausen, D., Wirth, M., Fix, A., Ehret, G., Knippertz, P., Toledano, C., Gasteiger, J., Garhammer, M. and Seefeldner, M.: Depolarization ratio profiling at several wavelengths in pure Saharan dust during SAMUM 2006, Tellus, Ser. B Chem. Phys. Meteorol., 61, 165–179, doi:10.1111/j.1600-0889.2008.00396.x, 2009.

Groß, S., Tesche, M., Freudenthaler, V., Toledano, C., Wiegner, M., Ansmann, A., Althausen, D. and Seefeldner, M.: Characterization of Saharan dust, marine aerosols and mixtures of biomass-burning aerosols and dust by means of multi-wavelength depolarization and Raman lidar measurements during SAMUM 2, Tellus, Ser. B Chem. Phys. Meteorol., 63, 706–724, doi:10.1111/j.1600-0889.2011.00556.x, 2011.

Heintzenberg, J., Birmili, W., Otto, R., Andreae, M. O., Mayer, J.-C., Chi, X. and Panov, A.: Aerosol particle number size distributions and particulate light absorption at the {ZOTTO} tall tower ({S}iberia), 2006–2009, Atmos. Chem. Phys., 11(16), 8703–8719, doi:10.5194/acp-11-8703-2011, 2011.

Mamouri, R. E., Ansmann, A., Nisantzi, A., Kokkalis, P., Schwarz, A. and Hadjimitsis, D.: Low Arabian dust extinction-to-backscatter ratio, Geophys. Res. Lett., 40, 4762–4766, doi:10.1002/grl.50898, 2013.

Mattis, I., Ansmann, A., Müller, D., Wandinger, U. and Althausen, D.: Multiyear aerosol observations with dual-wavelength Raman lidar in the framework of EARLINET, J. Geophys. Res., 109(D18), 13203, doi:10.1029/2004JD004600, 2004.

Mona, L., Amodeo, A., Pandolfi, M. and Pappalardo, G.: Saharan dust intrusions in the Mediterranean area: Three years of Raman lidar measurements, J. Geophys. Res. Atmos., 111, doi:10.1029/2005JD006569, 2006.

Müller, D., Ansmann, A., Mattis, I., Tesche, M., Wandinger, U., Althausen, D. and Pisani, G.: Aerosol-type-dependent lidar ratios observed with Raman lidar, J. Geophys. Res., 112, 16202, doi:10.1029/2006JD008292, 2007.

Nisantzi, A., Mamouri, R. E., Ansmann, A. and Hadjimitsis, D.: Injection of mineral dust into the free troposphere during fire events observed with polarization lidar at Limassol, Cyprus, Atm. Chem. Phys., 14(22), 12155–12165, doi:10.5194/acp-14-12155-2014, 2014.

Papayannis, A., Amiridis, V., Mona, L., Tsaknakis, G., Balis, D., Bösenberg, J., Chaikovski, A., De Tomasi, F., Grigorov, I., Mattis, I., Mitev, V., Müller, D., Nickovic, S., Pérez, C., Pietruczuk, A., Pisani, G., Ravetta, F., Rizi, V., Sicard, M., Trickl, T., Wiegner, M., Gerding, M., Mamouri, R. E., D'Amico, G. and Pappalardo, G.: Systematic lidar observations of Saharan dust over Europe in the frame of EARLINET (2000-2002), J. Geophys. Res. Atmos., 113, doi:10.1029/2007JD009028, 2008.

Pappalardo, G., Amodeo, A., Apituley, A., Comeron, A., Freudenthaler, V., Linné, H., Ansmann, A., Bösenberg, J., D'Amico, G., Mattis, I., Mona, L., Wandinger, U., Amiridis, V., Alados-Arboledas, L., Nicolae, D. and Wiegner, M.: EARLINET: towards an advanced sustainable European aerosol lidar network, Atmos. Meas. Tech., 7(8), 2389–2409, doi:10.5194/amt-7-2389-2014, 2014.

Ramanathan, V., Crutzen, P. J., Lelieveld, J., Mitra, A. P., Althausen, D., Anderson, J., Andreae, M. O., Cantrell, W., Cass, G. R., Chung, C. E., Clarke, A. D., Coakley, J. A., Collins, W. D., Conant, W. C., Dulac, F., Heintzenberg, J., Heymsfield, A. J., Holben, B., Howell, S., Hudson, J., Jayaraman, A., Kiehl, J. T., Krishnamurti, T. N., Lubin, D., McFarquhar, G., Novakov, T., Ogren, J. A., Podgorny, I. A., Prather, K., Priestley, K., Prospero, J. M., Quinn, P. K., Rajeev, K., Rasch, P., Rupert, S., Sadourny, R., Satheesh, S. K., Shaw, G. E., Sheridan, P. and Valero, F. P. J.: Indian Ocean Experiment: An integrated analysis of the climate forcing and effects of the great Indo-Asian haze, J. Geophys. Res., 106(D22), 28371–28398, doi:10.1029/2001JD900133, 2001.

Raut, J. C. and Chazette, P.: Assessment of vertically-resolved PM10 from mobile lidar observations, Atmos. Chem. Phys., 9, 8617–8638 [online] Available from: http://www.mendeley.com/research/assessment-verticallyresolved-pm10-mobile-lidar-observations/, 2009.

Royer, P., Chazette, P., Lardier, M. and Sauvage, L.: Aerosol content survey by mini N2-Raman lidar: Application to local and long-range transport aerosols, Atm. Env., 45, 7487–7495, doi:10.1016/j.atmosenv.2010.11.001, 2011.

Royer, P., Raut, J.-C., Ajello, G., Berthier, S. and Chazette, P.: Synergy between CALIOP and MODIS instruments for aerosol monitoring: application to the Po Valley, Atm. Meas. Tech., 3, 893–907, doi:10.5194/amt-3-893-2010, 2010.

Schuster, G. L., Vaughan, M., MacDonnell, D., Su, W., Winker, D., Dubovik, O., Lapyonok, T. and Trepte, C.: Comparison of CALIPSO aerosol optical depth retrievals to AERONET measurements, and a climatology for the lidar ratio of dust, Atm. Chem. Phys., 12, 7431–7452, doi:10.5194/acp-12-7431-2012, 2012.

Lidar profiling of aerosol optical properties from Paris to Lake Baikal (Siberia)

E. Dieudonné[1,*], P. Chazette[1], F. Marnas[1], J. Totems[1] and X. Shang[1]

[1]{Laboratoire des Sciences du Climat et de l'Environnement (LSCE), CEA / CNRS / UVSQ, Gif-sur-Yvette, France}

[*]{Now at Laboratoire de Physico-Chimie de l'Atmosphère (LPCA), Université du Littoral, Côte d'Opale, Dunkerque, France}

Correspondence to: E. Dieudonné (elsa.dieudonne@univ-littoral.fr)

Abstract

In June 2013, a ground-based mobile lidar performed the ~10,000 km ride from Paris to Ulan-Ude, near Lake Baikal, profiling for the first time aerosol optical properties all the way from Western Europe to central Siberia. The instrument was equipped with N_2-Raman and depolarization channels that enabled an optical speciation of aerosols in the low and middle troposphere. The extinction-to-backscatter ratio (also called lidar ratio or LR) and particle depolarization ratio (PDR) at 355 nm have been retrieved. The LR in the lower boundary layer (300-700 m) was found to be 63 ± 17 sr in average during the campaign with a distribution slightly skewed toward higher values that peaks between 50 and 55 sr. Although the difference is small, PDR values observed in Russian cities (>2 %, except after rain) are systematically higher than the ones measured in Europe (<1 %), which is probably an effect of the lifting of terrigenous aerosols by traffic on roads. Biomass burning layers from grassland or/and forest fires in southern Russia exhibit LR values ranging from 65 to 107 sr and from 3 to 4 % for the PDR. During the route, desert dust aerosols originating from the Caspian and Aral seas regions were characterized for the first time, with a LR (PDR) of 43 ± 14 sr (23 ± 2 %) for pure dust. The lidar observations also showed that this dust event extended over 2300 km and lasted for ~6 days. Measurements from the Moderate Resolution Imaging Spectrometer (MODIS) show that our results are comparable in terms of aerosol optical thickness (between 0.05 and 0.40 at 355 nm) with the mean aerosol load encountered throughout our route.

1 Introduction

The quantification of the aerosol radiative forcing still suffers from large uncertainties, making aerosols the dominant contribution in uncertainties on the anthropogenic influence on climate (IPCC, 2013). To improve the performance of climate models, observations are needed in order to provide better constraints from the regional to the global scale. Large observational networks such as the Aerosol Robotic Network (AERONET; Holben et al., 1998), the Micropulse Lidar Network (MPLNET; Welton et al., 2001) or the Aerosol, Clouds and Trace gases Research Infrastructure Network (ACTRIS, formerly EARLINET; Pappalardo et al., 2014) provide the long-term measurement series needed to build a climatology of aerosol optical properties at the continental and global scales.

Complementarily, numerous large field experiments have taken place over the past years to monitor long-range transport of aerosols and cover areas that do not host dense observation networks like oceans, South-East Asia, Africa or Arctic: for instance the Aerosol Characterization Experiments (ACE-1, ACE-2, ACE-Asia; Bates et al. 1998; Raes et al. 2000; Huebert et al. 2003), the Indian Ocean Experiment (INDOEX, Ramanathan et al., 2001), the African Monsoon Multidisciplinary Analysis (AMMA; Lebel et al., 2010), or the Polar study using Aircraft, Remote sensing, surface measurements and models, of Climate chemistry, Aerosols and Transport project (POLARCAT; Law et al., 2014). During those field campaigns, airborne measurements have been performed, which offer observations on a larger scale than fixed ground-based stations.

On a smaller, regional scale, field experiments took place near large pollution hotspots like Mexico City, with the Megacity Initiative: Local And Global Research Observations project (MILAGRO, Molina et al., 2010), or Paris, with the Air Pollution Over the Paris Region project (ESQUIF, Vautard et al., 2003; Chazette et al., 2005), the Lidar pour la Surveillance de l'Air (LISAIR, Raut and Chazette, 2007) and the Megacities: Emissions, urban, regional and Global Atmospheric Pollution and climate effects, and Integrated tools for assessment and mitigation project (MEGAPOLI, http://megapoli.dmi.dk/; Royer et al., 2011). Aerosol optical properties have thus been extensively documented over Western Europe and North America. Besides, Asia has drawn a growing attention as this region is becoming a larger contributor to aerosol anthropogenic emissions.

Conversely, very few measurement programs exist over Russia, which for instance hosts only five stable AERONET stations while the country covers 11.5% of the world's dry lands and contribute to aerosol emissions through large forest fires and several pollution hotspots like Moscow (12 million inhabitants) or large industrial cities. Some measurement stations exist like the ZOTTO tower, located in the taiga 600 km North-West of Krasnoyarsk, where CO, particle concentration and aerosol optical properties are measured continuously up to 300 m a.g.l. (Above Ground Level) since 2006 (Heintzenberg et al., 2013). Vertical profiles of particle concentration and extinction up to 5 km have been collected in the Tomsk region during an intensive flight campaign in 1986-1988, and then from monthly flights between 1999 and 2007 (Panchenko et al., 2012). At a larger scale, CO and particle concentrations have been measured during transcontinental flights in the framework of the Airborne Extensive Regional Observations in Siberia project (YAK-AEROSIB, Paris et al., 2010).

However, most of the resulting observations took place in the free troposphere, and the flight plan was aimed towards the remote Northern Siberian regions rather than the industrial cities of Southern Siberia.

For other regions, and particularly for the industrial cities of Southern Siberia, only space-borne instruments offer a regular coverage, for instance the Moderate Resolution Imaging Spectrometer (MODIS, e.g. King et al., 1992; Salomonson et al., 1989) or the Polarization and Directionality of the Earth Reflectance / Polarization and Anisotropy of Reflectances for Atmospheric Sciences coupled with Observations from a Lidar (POLDER / PARASOL, e.g. Deuzé et al., 2001) or the Cloud-Aerosol Lidar and Infrared Pathfinder Satellite Observation (CALIPSO, e.g. Winker et al., 2003 or Chazette et al., 2010). However, observations are limited by cloud coverage and by the satellite overpass time, so that ground-based observations are welcome to better document aerosols over Russia.

In June 2013, we performed the first road transect through Europe and Russia for aerosol profiling, with a N_2-Raman lidar instrument embedded on a van going all the way from Paris to Lake Baikal, where the season of forest fires had begun. This campaign offers a unique snapshot of aerosol optical properties from Western Europe to Eastern Russia, which can be extrapolated in a broader climatological context through satellite observations. This article aims at presenting the general variability of the aerosol nature, amount and optical properties along the journey. For this purpose, a systematic data processing is used, which precision is limited by the need to apply it both to the nighttime and daytime, noisier data. For this reason a finer characterization of the optical properties of the desert dust and biomass burning aerosols encountered in Russia is also presented, based on a few case studies using best quality data.

Therefore, this paper is organized as follows. Section 2 presents the itinerary of the campaign, the lidar instrument and the data processing methods used to retrieve the aerosol extinction, extinction to backscatter ratio or Lidar Ratio (LR) and Particle Depolarization Ratio (PDR). Then, Section 3 presents the variability of aerosols along the journey, the particle nature being identified through the combination of the two intensives properties that are the LR and PDR. Section 3 also analyzes the representativeness of the observations in regards to longer time series of space-borne measurements. Finally, Section 4 presents a few case studies on which it was possible to perform a finer characterization of the optical properties (LR and PDR) of the

dust and biomass burning particles encountered during the route, and the origin of those particles is also discussed.

2 Experimental setup and method

2.1 Itinerary

The van carrying the lidar instrument departed from Paris on June 4th 2013 and reached Lake Baikal on June 28th. The trip was performed during the summer as it corresponds to the maximum of the wildfire season. After June 28th, fixed location measurements were performed on the shore of Lake Baikal, in Istomino village (52.128°N, 106.287°E), and mobile observations were recorded during round trips between Istomino and Ulan-Ude city, 80 km South-East of the Lake. Ground-based mobile measurements, though limited by battery power, could be conducted during most of the journey (during daytime). Fixed location measurements took place during most of the stop-overs (during nighttime) using local power supply. Intermissions were thus mainly due to rain showers and low-level clouds.

An overview of the van itinerary and of the lidar data availability can be found on Figure 1. The journey went through a number of pollution hotspots: Paris, the Rhine Valley (Frankfurt), Berlin, Warsaw, Moscow, and several large and industrial Russian cities such as Nizhniy-Novgorod, Kazan, Ufa, Chelyabinsk, Omsk, Novosibirsk, Krasnoyarsk and Irkutsk. Regarding wildfires, three main vegetation types susceptible to produce biomass burning aerosols were encountered: first, temperate forest (visible in dark green on the MODIS image) dominate in the Baltic countries and Western Russia, then the vegetation turns into grasslands (lighter shades of green on the MODIS image) in the steppes of Southern Russia (i.e. from Nizhniy-Novgorod to Omsk, except in the Ural Mountains) and finally boreal forest occupies all the eastern part of the journey (and the Ural Mountains between Ufa and Chelyabinsk). The map is extended down to 40°N in order to show the desert areas in the Caspian and Aral seas region where the dust particles observed during the campaign originated from.

2.2 Instrumentation

The lidar instrument used during the campaign is similar to the one previously described by Royer et al. (2011). It operates at 355 nm with 16 mJ pulse energy, and has three acquisition channels for elastic, perpendicularly-polarized and N_2-Raman backscatters. The signals were recorded with an initial resolution of 25 s (500 laser shots) and 0.75 m, both in analog and

photon-counting mode. During daytime, when the photodetectors are saturated by the sky background light, only the analog mode is used, whereas during nighttime the analog and photon-counting signals are merged to optimize both dynamic range and signal-to-noise ratio. After correction for the platform inclination (measured using a Xsens MTi-G GPS/inclinometer attached to the optical head) and after cloud screening, data are averaged over 5 or 30 minutes and 7.5 m in altitude. The 30-minute averaging period was chosen because it makes the signal from the N_2-Raman channel exploitable up to 700 m, even during daytime, without mixing data recorded in too distant locations (~50 km given the speed limits).

The overlap functions of the lidar channels were assessed before the trip using horizontal profiles, when the lower atmosphere could be considered as homogeneous along the line of sight. Once attached to the van, it was not possible to tilt the lidar to retrieve the overlap function from a horizontal profile. It was instead checked using fixed observations below fair weather afternoon cumulus clouds (i.e. in a supposedly homogeneous boundary layer). The overlap function retrieved at different points of the journey (Riga, Irkutsk, Istomino) is remarkably similar, which confirms the optical stability and validates the well-mixed boundary layer hypothesis. Complete overlap is reached between 250 and 300 m a.g.l.

2.3 Retrieval of the aerosol extinction and lidar ratio

The signal from the N_2-Raman channel is used to derive the aerosol optical depth profile supposing a constant value of 1 for the Angstrom exponent (Ångström, 1964). Indeed, only sun-photometers provide Angstrom values in the UV wavelengths (MODIS only provides the Angstrom exponent between its 470 and 660 nm channels) and the van journey came close to only four AERONET stations over the 10,000 km. In the absence of experimental data, using an average value of 1 appears as a good compromise (the residual relative uncertainty was calculated to be less than 3 % by Chazette et al., 2014). Also, molecular diffusion is corrected using extinction and backscatter profiles determined using a reference atmospheric density profile and a polynomial interpolation between the 40 levels of this profile (Royer et al., 2011 and references therein). Then, two data processing methods are used, depending on whether the Raman optical depth profile reaches an aerosol-free layer or not.

2.3.1 Systematic data processing

To analyze the variability of aerosols along the journey, we wish to obtain a set of aerosol optical thicknesses (AOT), lidar ratio (extinction-to-backscatter ratio, LR), and particle depolarization ratio (PDR) values using a systematic processing performed on the 30-minute average profiles from the whole campaign (day- and night-time). However, as the range of the N_2-Raman channel is limited by the sky background light during daytime, this processing can only rely on a partial AOT between 300 m (complete overlap) and 700 m a.g.l. (range limit of the N_2-Raman channel at noon). The partial AOT from the Raman channel serves to constrain the lidar ratio used in a standard Klett inversion (Klett, 1985), which is achieved through a convergent process described in Appendix A. When convergence is reached, the retrieved value corresponds to the average lidar ratio in the 300-700 m a.g.l. layer. The uncertainty on this value is estimated by propagating the photon noise on the lidar signal throughout the inversion process using a Monte-Carlo algorithm. A profile is considered as "fully convergent", and the retrieved lidar ratio is considered as valid, only when all the 200 profiles in the Monte-Carlo distribution are convergent.

Unfortunately, the partial AOT produced by the Klett inversion is very sensitive to the transmission by the upper layers, making convergence difficult when another aerosol type with a different LR is present above the constraint layer (e.g. an elevated dust or biomass burning layer or more frequently, moist aerosols near the PBL top). Consequently, only a small fraction of the profiles converge (see Sec. 3.1); for the others, it is necessary to choose an arbitrary LR value in order to compute the extinction profile, total AOT, and subsequently the PDR. In order to avoid introducing discontinuities in the AOT and PDR datasets between profiles that converged or not, the same LR value is used to invert all profiles through a standard Klett procedure. The chosen LR (58 sr) is the mean value of the LR distribution obtained from the valid profiles (see Sec. 3.1).

2.3.2 Case study data processing

The case studies presented in Section 4 rely on fixed measurements, with longer time averaging. Nighttime observations, added to this longer averaging, make the N_2-Raman channel exploitable up to a purely molecular layer (above 6 km a.g.l). In this case, a complete lidar ratio profile can be retrieved using either the standard Raman inversion method described in Ansmann et al. (1990) or a constrained Klett method similar to the one used for the systematic processing, but applied on a sliding window browsing the full altitude range.

More details about both inversion processes are given in Appendix A. After the LR profile has been retrieved from the average profile over the whole period, it is used to process more frequent 5-minute average profiles and invert the time-dependent extinction profile and AOT.

2.4 Retrieval of the Particle Depolarization Ratio (PDR)

The volumetric depolarization ratio (VDR) was determined following the procedure described in Chazette et al. (2012). It uses the transmission and reflection coefficients of the polarization separation plates as measured in the lab before departure, along with the gain ratio between the total and perpendicular polarization channels. The gain ratio value was calibrated using measurements obtained next to Lake Baikal during one night when the atmosphere was devoid of any elevated aerosol layer, featuring a purely molecular depolarization (with a value known from the filters bandwidth). Several tests carried on other days earlier during the campaign showed that the gain ratio varied by 5 % at most, so that the value obtained from the Lake Baikal experiment was used during the whole campaign. The particulate depolarization ratio (PDR) is then computed as in Chazette et al. (2012). As the PDR is a physical parameter without meaning when there are few aerosols, its calculation is performed only for layers where the aerosol backscatter coefficient is at least 5 % of the molecular backscatter (i.e. a scattering ratio above 1.05).

The error on the PDR is computed for each case presented in this study. The values and dominant sources of error are discussed in Appendix B. Below 4 km a.g.l, we find that, given the chosen scattering ratio threshold of 1.05, the relative uncertainty on the PDR is largely constrained by the uncertainty on the lidar ratio (i.e. between 8% and 20% – relative) for PDR values of 5% and above. Because of the error on the gain ratio, this relative uncertainty is always at least 7%. For very low PDR values, the absolute uncertainty mostly depends on noise conditions, but remains above 0.2%. More details and about the validation of these values via Monte-Carlo simulation are given in Appendix B.

3 Variability of aerosols along the transect

All this section is based on the 30-minute average profiles inverted using the systematic processing described in Section 2.3.1. First, the distribution of LR values retrieved in the planetary boundary layer (PBL) is presented. Then, the spatial distribution of aerosols along the journey, analyzed in terms of AOT and PDR, is discussed. A finer classification of the particle types encountered during the campaign is also proposed, based on the LR and PDR

values retrieved in the PBL. Finally, the representativeness of the campaign period is assessed by comparison with longer time series of space-borne observations and ground-based sun-photometers.

3.1 Distribution of lidar ratios in the boundary layer

Data recorded during the whole campaign produced 547 cloudless 30-minute average profiles. Because of sometimes unsufficient aerosol load or due to the presence of elevated aerosol layers, only 106 profiles (~19 %) can be considered as "fully convergent" i.e. they give the best quality LR values (see Sec. 2.3.1). Among those 106 convergent profiles, 30 (~28 %) are located in Istomino village as several days of observations have been recorded there between June 29th and July 7th 2013. In order not to give the Baikal region an excessive weight, the LR distribution is computed on the 76 profiles recorded elsewhere than Istomino village (Figure 2). LR values during the campaign range from 32 to 106 sr, with an average and standard deviation of 63 ± 17 sr; the distribution is slightly skewed towards high values (median LR is 61 sr and first / last quartiles are 51 / 74 sr). In Istomino village, the distribution (not shown) exhibits higher and more scattered values (average / standard deviation of 70 ± 20 sr) associated with a generally low aerosol load observed near Lake Baikal (the average AOT was only 0.07 at 355 nm).

A sample of the lidar ratio observations available in the literature for different types of aerosols is presented in Table 1 (desert dust), Table 2 (biomass burning) and Table 3 (anthropogenic pollution). It show that the LR distribution observed during the Paris-Baikal journey is compatible with previous observations for pollution aerosols, aged smoke and mixes with terrigenous particles (dust), which are the types of aerosol that can be expected in such continental conditions.

In the following parts of Section 3, the 30-minute average profiles are processed using Klett's inversion with a constant LR of 58 sr when considering the entire atmospheric column. For specific study in the PBL, between 300 and 700 m, the N_2-Raman Chanel was used to assess LR.

3.2 Classification of aerosols along the route

In order to discuss the distribution of aerosols along the transect, Figure 3 presents the Aerosol Optical Thickness (AOT) and Particle Depolarization Ratio (PDR) inverted from all

the 30-minute average profiles, plotted against longitude. Profiles recorded within a radius of 15 km are grouped and replaced by their average, which leaves 122 profiles. To discuss the vertical distribution of aerosols, the partial AOT and the average PDR below and above a fixed level are computed. An altitude of 1500 m a.g.l. was chosen as it can be considered as an average value for continental PBL or residual layer top, i.e. the maximum altitude influenced by the ground. Values of PDR above 1500 m a.g.l. are scarce because this ratio cannot be computed for profiles gathered around noon (the depolarization channel SNR is too low) or when the aerosol load is too small in the free troposphere.

To obtain more insight into the type of aerosols encountered during the route, the scatter plot of PDR vs LR values in the PBL (300-700 m a.g.l.) is presented on Figure 4. The uncertainty on the LR values is the standard deviation of the LR distribution provided by the Monte-Carlo algorithm. The uncertainty on the PDR value is computed following the process described in Appendix B. Dots are colored according to their geographic origin. In Russia, profiles were split between urban and background cases, the "urban" criterion being a longitude difference smaller than 0.5° with the city center. Profiles were also split between the dust event zone (longitude from 45 to 75°E) and the rest of the country. Cities in the dust zone are Kazan, Ufa, Chelyabinsk and Omsk (Ishim is not included because too small); other Russian cities are Pskov, Moscow, Nizhniy-Novgorod, Novosibirsk, Irkutsk and Ulan-Ude (Nizhneudinsk is not included because too small). Krasnoyarsk was analyzed separately.

European part of the route. Aerosols from Europe (longitude < 26°E, red dots in Figure 4) are characterized by rather high LR and low PDR values (60-102 sr and <1 %) indicating the predominance of spherical carbonaceous particles (pollution aerosols). This is the case for large cities such as Paris and Berlin. PDR values in the rural regions of Central Germany are slightly higher (< 2 %). Over Germany and Poland (particularly near Frankfurt, Berlin and Warsaw), higher values of free tropospheric AOT show the presence of elevated aerosols layers with PDR values similar to those found in the PBL, suggesting that this is probably pollution lifted up and transported from another part of Europe.

Russian part of the route. In Russian cities (black and orange dots in Figure 4), the urban PBL is generally characterized by slightly higher PDR values (2-4 %) as compared to Europe, which indicates that the particle composition results from a mixture of traffic and industrial emissions with terrigenous aerosols. Russian cities East of Moscow appear much dustier than European cities due to bad road tarmac and lack of vegetation on traffic islands, which results

in a lot of terrigenous aerosols being lifted up by the wind and by road traffic and injected in the urban PBL. The large dispersion of LR values may be due to a strong variability of aerosol types. Krasnoyarsk is the only one city where PDR values are comparable with European cities (yellow dots in Figure 4) but this is probably not due to a difference in the aerosol sources. Indeed, heavy rain had fallen during the night before the van went through the city and the ground was still wet, proving that the terrigenous aerosol had all been washed down. Between Krasnoyarsk and Nizhneudinsk, AOT values up to 0.28 have been observed (Figure 3), with a large fraction located in the free troposphere (up to 47 %). As they are associated with very low values of PDR (<1 %), both below and above 1500 m a.g.l., it could either be pollution aerosols transported from the industrial city of Krasnoyarsk, or more probably part of a forest fire plume.

Desert dust in Russia. The values of PDR > 10 % (Figure 3) between Kazan and Ufa (~52°E) correspond to a desert dust event, with first, an elevated layer (PDR ~35 %) and then, mixing of the dust into the PBL (PDR ~17 %). The highest AOT values (up to 0.40, associated with up to 70 % of the AOT above 1500 m a.g.l.) were observed farther East, between Ishim and Omsk (~71°E). However, the PDR values (5-9 %) indicate that a mixing has occurred with combustion aerosols, most probably of biomass burning origin since the region is very isolated. Indeed, combustion aerosols from pollution or biomass burning are found with PDR values below 5 % at 355 nm while aerosol mixes dominated by dust-like particles usually have PDR values above 10 % and pure desert dust above 20 % (see references in Table 1, Table 2 and Table 3).

The PDR values of ~35 % found between Kazan and Ufa (Figure 3, lower panel) are very high for dust but they were derived using the campaign average LR in the PBL, not with a dust optimized LR value, which results in large uncertainties. Besides, values of 38 % have already been observed at 355 nm in volcanic ash plumes (Ansmann et al., 2011). Russian cities located in the area where elevated layers of dust were observed (orange dots in Figure 4) do not show a different distribution of LR and PDR compared to other Russian cities (black dots). This indicates that the mixing of the elevated dust layers towards the PBL was low, or that its effects were limited as the LR values were already affected by terrigenous aerosols from local sources lifted in the PBL.

Background aerosols. In unpopulated areas of Russia, aerosols are probably a mix between aged particles from biomass burning and secondary organic aerosols, so that very low

depolarization can be expected when no dust is present (PDR < 1%). Also, under local terrigenous aerosol source-free conditions, the dust plume has a more sensible effect on the PDR than in town. LR values in remote areas are rather low (32-50 sr). However, in the absence of dust, the AOT values used as constraint are small and result in large uncertainties on the LR values. Note that the smallest AOT values (below 0.1 at 355 nm, Figure 3) were derived between Pskov and Smolensk (West of Moscow) and in Siberia between Omsk and Novosibirsk, and close to Istomino village, on the shore of Lake Baikal (between Irkutsk and Ulan-Ude). They correspond to periods interspersed with rain.

3.3 Temporal representativeness of the observations

The lidar-derived AOT values presented in Section 3.1 were compared with the AOT measured by MODIS Terra. A multi-year average was computed from the monthly 1°×1° gridded product (MOD08_M3) using the months of June from years 2000 to 2013 (only years 2001, 2003 and 2012 were removed because, due to intense fire events, those years are too far from the conditions encountered during the campaign). MODIS data from the grid pixel where the lidar was located were extracted without any spatial interpolation. For the four AERONET stations located close to the transect (Palaiseau, Mainz, Moscow and Irkutsk), monthly averages were computed from the daily averages including at least 4 observations, then the multi-year June average was computed from years 2006 to 2013 (the time period is shorter than for MODIS because Mainz and Irkutsk records started in 2006). The AOT values were all converted to 355 nm using the Angstrom coefficients provided by MODIS and AERONET. The resulting AOT values for the lidar, MODIS and AERONET, are presented in Figure 5. (top panel).

The lidar-derived AOT stays within a 1-σ interval around the MODIS multi-annual June average during most of the journey. The largest deviation from MODIS average was observed between Ishim and Omsk, due to the mixed dust and biomass burning event identified in Section 3.2. The pure dust layers observed near Kazan, as well as the fire or pollution layers observed near Nizhneudinsk are associated with moderate AOT values, which remain close to the MODIS average. However, the MODIS daily 1°×1° product (not shown) displays AOT values larger than the lidar observations (up to 0.6), suggesting that we did not sample the heart of the plumes. Elsewhere, AOT values standing clearly below MODIS highlight the areas where we observed background aerosols, i.e. between Pskov and Smolensk (~30°E, West of Moscow), between Omsk and Novosibirsk (~80°E) and in Central Germany (Leipzig

area). This AOT comparison shows that our observations are representative of the aerosol load existing above Europe and Russia in June, in the absence of exceptional fire or dust events.

In middle and bottom panels of Figure 5. , the blue curves (green dots) represent respectively the 470-660 (440-675) nm Angstrom coefficient and the 550 (500) nm AOT fine mode fraction from MODIS Terra (AERONET). The average and standard deviation have been computed the same way as the AOT. The drop in MODIS AOT around 23°E (Poland-Lithuania border) is correlated with an increase of the Angstrom coefficient and of the fine mode fraction, indicating that the aerosol mix in Russia contains more small particles than in Europe, which is in apparent contradiction with the observations of our lidar highlighting the presence of a larger fraction of coarse terrigenous particles over Russia.

However, this discrepancy probably results from the differences in the observation scales. The LR and PDR values observed by the lidar indicate the presence of coarse terrigenous aerosols in the lower PBL (300-700 m a.g.l.) and nearby the road followed by the van, which is one of the busiest of Russia with heavy truck traffic. On the other hand, MODIS represents an average over the whole atmospheric column and a large land surface (111 × 64 km^2 at 55°N) so it is more representative of the free troposphere and of the rural areas of Russia, where the aerosol mixture is dominated by biomass burning particles. Only in Moscow, where the city is large enough to occupy a significant part of the 1°×1° pixel, MODIS exhibits a drop of the fine mode fraction down to European values. Those changes in the Angstrom coefficient and in the fine mode fraction are not visible on the sun-photometers data, maybe due to a difference between the aerosol models used in AERONET and MODIS retrievals.

4 Characterization of dust and biomass burning aerosols events

This section presents case studies of dust or biomass burning aerosol plumes during which a finer characterization of the optical properties of these particles was possible through the retrieval of their lidar ratio using a Raman or multi-layer constrained Klett inversion. The origin of the particles is also studied for each aerosol plume. Finally, we discuss our results taking into account the observations made in other regions of the world.

4.1 Case studies

4.1.1 Dust and biomass burning aerosols observed West of Kazan

The first significant observation of dust layers occurred near Kazan (49°E, 56°N) on June 18th 2013. The LR and PDR profiles are computed on a 55-minute average profile recorded just after sunset. Figure 6 presents the results from the Raman inversion and from the multi-layer constrained Klett inversion, along with the uncertainties computed through the Monte-Carlo process. The two inversions result in a very good agreement above 1.05 km a.m.s.l.; below this altitude, the constrained Klett procedure did not converge due to the low aerosol load, meaning the high LR values provided in this layer by the Raman inversion are not significant either. The uncertainties on the lidar ratio profiles are relatively large and come from the low signal-to-noise ratio (~20) due to an averaging time limited by cloud cover.

According to the particle depolarization (PDR) profile (Figure 6, right), the dust layer extends from 2.05 to 3.45 km a.m.s.l (average PDR of 19 ± 2 %). Compared to the references summarized in Table 1, the lidar ratios retrieved in the upper part of the layer (2.85-3.45 km a.m.s.l.) are typical of pure dust: 48 ± 16 sr (43 ± 14 sr) for the Raman inversion (resp. constrained Klett inversion). In the lower part of the layer (2.05-2.85 km a.m.s.l.), the lidar ratio values are 78 ± 12 sr (75 ± 9 sr) for the Raman inversion (resp. constrained Klett inversion), which suggests a mix between dust and biomass burning aerosols within the atmospheric column. Indeed, below the dust layer, the PDR drops down to values <10 % that are typical for smoke (see references in Table 2). The lidar ratios in this layer also point toward combustion particles, though the values are higher than what is reported in the literature, with 107 ± 14 sr for both inversion methods (1.05-2.05 km a.m.s.l. average).

The temporal evolution of this event is studied using 5-minute average profiles. The inversion is performed using the LR profile derived from the constrained Klett procedure. The resulting AOT, aerosol backscatter coefficient and PDR are presented on Figure 7. The AOT is slightly lower than the values provided by MODIS Aqua (~0.5), but the satellite overpass took place at 9:20 UTC, i.e. 8 to 9 hours before the lidar observations. Moreover, the map of MODIS AOT (not shown) indicates that we sampled the eastern edge of the plume, which is confirmed by the decreasing AOT values observed as the van moves eastwards.

The backscatter and PDR time-height cross-sections show that the dust layer became thinner from 17:30 UTC and moved upwards (Figure 7, middle and bottom panels). As the profile

used for LR retrieval is an average between 17:29 and 18:24 UTC, this explains why the LR values below 2.85 km a.m.s.l. correspond to a dust-smoke mix. On the contrary, the time-height cross-sections show that dust remains present above 2.85 km a.m.s.l. and confirm that the LR of 43 ± 14 sr retrieved in this layer can be attributed to pure dust. The PDR reaches values of ~23 ± 2 % in the heart of the layer (average from 17:15 to 17:45 UTC and between 2.05 and 2.85 km a.m.s.l.), which is close to other observations at 355 nm for pure dust (Table 1; Groß et al., 2011; Müller et al., 2012). In the biomass burning layer (1.05-1.4 km a.m.s.l.), the PDR is ~4 ± 2 % on average while it is ~13 ± 3 % in the dust-smoke mix (after 18 UTC, 2-2.8 km a.m.s.l.).

4.1.2 Dust and biomass burning aerosols observed above Omsk

Omsk is one of Russia's largest industrial centers and a 1.15-million inhabitant city located 2300 km East of Moscow (55°N, 73°E). Several oil and gas fields are exploited north of the city, whose industry is dominated by hydrocarbon production. The van was stationed in the center of the city, near the Irtysh River, during the night from June 22nd to 23rd.

Observations show the successive overpass of a dust layer and a biomass burning layer over the van. To retrieve the lidar ratio, two average profiles were computed: one that samples the dust layer (16:44-19:12 UTC) and one during the overpass of the biomass burning layer (19:12-21:42 UTC). Figure 8 presents the LR profiles computed using the Raman inversion and the multi-layer constrained Klett inversion. In the heart of the dust layer (left profile, 2.5-3.5 km a.g.l.), the average LR is 50 ± 11 sr (54 ± 11 sr) according to the Raman inversion (resp. constrained Klett inversion), which is close to the layer observed near Kazan and typical of pure desert dust aerosol (references in Table 1). In the biomass burning layer (right profile, 1.5-2.5 km a.g.l.), both inversion methods lead to an average LR of 76 ± 10 sr, a value that is compatible with the literature (references in Table 2).

In the residual layer (0.5-1.0 km a.g.l.), LR values increase during the night: for the Raman inversion, the average LR before 19 UTC (profile #1) is 67 ± 12 sr while it reaches 92 ± 18 sr after 19 UTC (profile #2). The values provided by the constrained Klett inversion are higher (79 ± 8 sr, then 101 ± 4 sr) and show less agreement with the literature (references in Table 3), the highest reported values being ~83 sr (Raut and Chazette, 2007; Royer et al., 2010, 2011). This increase in LR is possibly due to a change in the aerosol mix during the night: as the large terrigenous particles lifted from the road tarmac during the day return progressively

to the ground, highly absorbing pollution aerosols become dominant. Such an effect was also observed in Irkutsk (not shown).

The LR profiles retrieved from the constrained Klett inversion are used to invert the 5-minute average profiles; the resulting AOT, backscatter coefficient and PDR are presented on Figure 9. The decrease of AOT from 15 to 19 UTC stems mainly from the decrease of the particle extinction (and backscatter) in the residual layer after sunset, following the disconnection from fresh ground emissions. It goes along with a slight decrease of the average PDR below 1.2 km a.g.l. (from 4 ± 1 % before sunset to 3 ± 1 % after 18 UTC) also supporting the terrigenous fallout hypothesis. Those depolarization values are coherent with the classification of Burton et al. (2012), who reported 532 nm PDR values from 3 to 8 % for pollution aerosols, and with the observations of Müller et al. (2007), who always observed PDR values lower than 5 % for urban haze.

The backscatter and PDR time-height cross-sections show the existence of a second, thinner smoke plume moving upward just above the dust plume, which could explain why the average PDR is only 17 ± 2 % is the dust plume (16:45-19 UTC and 2.5-3 km a.g.l.). In the biomass burning plume, the average PDR is 4 ± 2 % (after 19:30 UTC and 1.6-2.6 km a.g.l.) with a zone where it drops to 2 ± 1 % (19:45-21 UTC and 1.5-2 km a.g.l.). The clean layer isolating the smoke plume from the residual layer is associated with a sharp wind shear visible on the reanalyzes from the European Center for Medium-range Weather Forecast (not shown). MODIS observations show that, again, the lidar sampled only the edge of the plume as the 355 nm AOT reached ~0.7 on June 22nd morning (Terra/Aqua, ~7:00 UTC) but only ~0.2 remained on June 23rd morning (Terra, 6:10 UTC), a value in agreement with the lidar AOT measured 5 hours earlier.

4.1.3 Additional cases

Two additional cases that cannot be detailed extensively are briefly described in this section; results are summarized in Table 1 and Table 2. One day before the Omsk case study (night from June 21st to 22nd), similar observations were recorded near the town of Ishim (65,000 inhabitants, 56°N, 69°E), with a dust layer after sunset (though too thin to properly determine an average LR and PDR) and a biomass burning layer during the second part of the night (LR of 65 ± 6 sr, PDR of 3 ± 1 %). Then, during the night from June 25th to 26th, the van halted in the small city of Nizhneudinsk (55°N, 99°E, 37,000 inhabitants). No dense layers of aerosols were visible but a diffuse background reached up to 3.5 km a.g.l., with an average LR of

63 ± 15 sr and an average PDR ~1 %. Dust plumes were also visible while the van travelled in between cities although daytime observations do not allow the quantitative determination of the LR and PDR for elevated layers. Those cases will therefore not be included in the discussion.

4.2 Origin of the elevated layers

To identify the dust sources, Figure 10 presents 7-day backward trajectories ending in the dust layer observed West of Kazan (Sec. 4.1.1). The trajectories have been calculated using the Hybrid Single Particle Lagrangian Integrated Trajectory Model (HYSPLIT 4, http://ready.arl.noaa.gov/HYSPLIT.php) under the isentropic mode for the vertical velocity. We used HYSPLIT in the ensemble mode, which is designed to assess the trajectory uncertainty by shifting the wind field at the ending point by one grid point in each of the 3 directions, giving 27 back-trajectories.

The fact that 20 of the back-trajectories do not enter the PBL during their journey shows that the air mass was mostly of free tropospheric origin, which is not surprising as MODIS already showed that the lidar sampled only the edge of the plume. Among the 7 remaining back-trajectories, ground contact occurred in the North-Western and central parts of Kazakhstan, in the Volga mouth region (North-West bank of the Caspian Sea) and in the area between the Caspian and Aral seas. MODIS true color reflectance (Figure 10 background) shows that the Caspian-Aral region is a desert area, and geological maps available from the European Soil Portal (http://eusoils.jrc.ec.europa.eu/library/esdac/index.html) confirm that large sandy areas stand at the South and East of the Aral Sea (Kyzylkum and Karakum deserts), and to a lesser extent at the North-West of the Caspian Sea. In the area between the Aral and Caspian seas, and also in large parts of central Kazakhstan, soils are of loamy type, even including clay deserts like in the Sahel ("takyr") or salt deserts ("solonchak"). Conditions for dust lifting are thus gathered in this region.

To identify the origin of the biomass burning particles observed along with the dust, MODIS fire hot-spots are also indicated on Figure 10 (MCD14ML product from the University of Maryland; Giglio et al., 2006). Fires coinciding with the back-trajectories are located in the steppes near the western Russian-Kazakh border and to the north-west of the Aral Sea. Regarding the possibility of those particles to actually be anthropogenic pollution, the cities of Saratov (51.5°N, 46°E, ~840,000 inhabitants) and Volgograd (49°N, 44°E, ~1 million

inhabitants) could have contributed. However, only a more detailed backward dispersion study could confirm this and meanwhile, a wildfire burning origin remains much more likely.

Figure 11 displays a similar ensemble of HYSPLIT 7-day back-trajectories, but ending in the dust layer observed above Omsk. Those trajectories confirm that it has the same origin as the dust layer observed near Kazan 5 days earlier, i.e. the sandy / loamy soils of south-western Kazakhstan. Incidentally, from Moscow (June 16th) to Omsk (June 22nd), the van travelled eastwards at the same pace as a high pressure system. As the winds curled around the anticyclone, air masses which had passed over the Caspian-Aral region were continuously brought up to the North, producing dust outbreaks over 2,300 km, from 38°E to 73°E. The weak and changing winds prevailing near the center of the anticyclone are also responsible for the erratic shape of the early part of the trajectories.

The back-trajectories (not shown) ending in the biomass burning layer observed above Omsk a few hours later are very similar to those presented on Figure 11. MODIS highlights three fire areas located in the steppes of north-western Kazakhstan (51°N-54°E, 50°N-56°E and 48°N-57°E) that had significant fire power (90 to 120 MW) and were overpassed at low altitude by the back-trajectories. Fires hot-spots were also observed by MODIS in the wooded area located under the latest part of the back-trajectories (60-62°N, 69-73°E). However, their fire radiative power is low (max. 38 MW) so that it is doubtful that the smoke was injected as high as the back-trajectories (~2 km a.g.l.). However, larger fires might have escaped the eyes of MODIS as the back-trajectories travelled along the southern edge of a cloud system.

Back-trajectories ending above Nizhneudinsk (not shown) indicate that the air mass came from the forests areas of the Far North but a dense cloud cover blinded MODIS and prevented the identification of the aerosol sources.

4.3 Discussion

To summarize, LR and PDR values from the different case studies are recalled in the lower part of Table 1 (desert dust) and Table 2 (biomass burning), along with the references they can be compared with.

4.3.1 Desert dust aerosols

Particle depolarization ratio. The 23 ± 2 % PDR retrieved in the Kazan dust layer confirms it was pure desert dust. Indeed, it falls in between the two values reported in the literature for

PDR at 355 nm which are ~20 % for Gobi desert dust advected over Tokyo (Murayama et al., 2004) and 25 ± 6 % in Saharan dust layers advected over Morocco and Cape Verde during the Saharan Mineral dust experiments (SAMUM; Groß et al., 2011; Müller et al., 2012). For mixes of desert dust with biomass burning ("dusty mixes"), the values retrieved near Kazan (13 ± 3 %) and above Omsk (17 ± 2 %) are difficult to compare as the PDR strongly depends on the proportions of the aerosol mix. Values of 18 ± 3 % have been reported during SAMUM (Groß et al., 2011; Müller et al., 2012), whereas Chazette et al. (2014) found 16 to 19 % in Saharan dust layers advected over the Balearic Islands during the Hydrological cycle in Mediterranean Experiment (HyMeX) campaign. Simultaneous observations at 355 and 532 nm during the SAMUM campaigns showed that the depolarization of desert dust aerosols increases with wavelength (Groß et al., 2011; Müller et al., 2012) so that the 28 to 35 % PDR values reported at 532 nm by Burton et al. (2012) and Mamouri et al. (2013) cannot be compared directly to our Russian observations.

Extinction-to-backscatter (lidar) ratio. The 355 nm LR values reported in the literature for pure desert dust range from 38 ± 5 sr for Saudi Arabian dust advected over the Maldives Islands during INDOEX (Müller et al., 2007) to 58 ± 7 sr for western Saharan dust during SAMUM (Müller et al., 2012). The observations during SAMUM also show a slight decrease of the lidar ratio from 355 to 532 nm (Müller et al., 2012). Indeed, the range of values at this wavelength is slightly lower, with 34 to 39 sr for Syrian dust advected over Cyprus (Mamouri et al., 2013) and 44 to 51 sr for an ensemble of airborne campaigns over North America and the Caribbean (Burton et al., 2012). The observations presented in this paper are therefore in good agreement, as we retrieved 43 ± 14 sr for pure desert dust (Kazan case) and 50 ± 13 sr for an aerosol mix containing a large fraction of dust, as indicated by its 17 % PDR (Omsk case). Schuster et al. (2012) showed that the lidar ratio of desert dust has a strong geographic dependency, following changes in the mineralogical composition of the dust particles. Our observations correspond to the LR values retrieved in the Sahel by Schuster et al. (2012). Unfortunately we cannot relate it to the mineralogical composition of dust particles in the Caspian-Aral region, as we could not find information on that point. Regarding dusty mixes, the comparison is difficult as the LR, like the PDR, will strongly depend on the proportions of dust in the mix; one can just note that the 75 ± 9 sr retrieved in the dust-smoke mix west of Kazan are identical to the SAMUM observations (Groß et al., 2011).

4.3.2 Biomass burning aerosols

Particle depolarization ratio. During this campaign, aged smoke plumes of two origins were sampled: particles coming from fires in the steppes or forests of northern Kazakhstan / southern Russia have PDR values of 3 to 4 %, whereas particles coming from forest fires in Far North Siberia have a very low PDR of ~1 % (Nizhneudinsk case). In the literature, depolarization ratios for aged smoke are 4-9 % (Burton et al., 2012), 5 ± 2 % (Tesche et al., 2011) or <5 % (Müller et al., 2007), for measurements that were all performed at 532 nm. No simultaneous observations of PDR at 355 and 532 nm exist for biomass burning aerosols, although measurement of a mixed smoke and dust layer suggest that the PDR does not vary much with wavelength (Groß et al., 2011). Therefore, the PDR values retrieved for smoke coming from Kazakhstan / southern Russia are in good agreement with the literature.

Particles from the Far North observed above Nizhneudinsk have a lower depolarization ratio than every observations reported. However, Nisantzi et al. (2014) showed that the depolarization of smoke layers strongly depends on their dust content, that will itself depend on the soil nature around the fire (as dust can be lifted by the eddies caused by the fire heat) and on the plume age (as the coarse dust particles will quickly fall out). This might explain why smoke from Kazakhstan, where the ground is semi-desert, exhibits a higher depolarization than smoke from northern Siberia. Besides, the low value of extinction in this plume indicates that the particle concentration is small, suggesting that, rather than the plume from a single large fire, this might result from a mix between smoke from several small scattered fires and biogenic aerosols (secondary organics) collected all along the air mass journey over the plains of northern Siberia.

Lidar ratio. Simultaneous observations at 355 and 532 nm showed a strong variability of the LR of biomass burning aerosols with wavelength (Müller et al., 2005; Murayama et al., 2004; Nicolae et al., 2013; Tesche et al., 2011) so our measurements will be compared preferentially with other observations at 355 nm. Amiridis et al. (2005) report a large dispersion of 355 nm LR values, from 39 to 94 sr, based on statistics over 4 years of smoke plumes from Russia and Ukraine advected above Greece. Other observations generally display LR values in the lower range of this interval: ~40 sr in a Siberian plume advected over Tokyo (Murayama et al., 2004), 46 ± 13 sr in Siberian and Canadian plumes advected over Germany (Müller et al., 2005) and 32 to 48 sr in plumes from Ukraine and Russia (Nicolae et al., 2013). However, 87 ± 17 sr (~100 ± 25 sr) have also been retrieved in an African smoke plume during

SAMUM (AMMA) by Tesche et al. (2011) (Chazette et al., 2007). Three of our observations are in good agreement with those references, i.e. the cases from Ishim (65 ± 6 sr), Omsk (76 ± 10 sr) and Nizhneudinsk (63 ± 15 sr). The 107 ± 14 sr observed west of Kazan is above all other observations but not incompatible with Amiridis et al. (2005) or Tesche et al. (2011) given the large uncertainty.

5 Conclusions

For one full month, a mobile N_2-Raman and depolarization lidar probed aerosols along the 10,000 km ride from Paris to Ulan-Ude (2 to 108°E, ~55°N). A systematic data-processing was performed on the 30-minute average profiles: the Raman channel was used to constrain the average extinction-to-backscatter ratio (i.e. lidar ratio or LR) between 300 and 700 m a.g.l. The campaign average LR was found to be 63 ± 17 sr along the journey and 70 ± 20 sr in the isolated village of Istomino (Lake Baikal shore). The distribution of the LR and particle depolarization ratio (PDR) values shows that aerosols in Europe are characterized by higher LR values (60-102 sr) and very low PDR (< 1 %) both in cities and in the countryside, indicating the dominance of pollution aerosols. In Russia, the LR values are more variable (44-106 sr) and a clear distinction exists between the countryside (PDR < 1 % as in Europe), and the cities (PDR > 2 %). The higher depolarization in Russian cities is likely due to the significant amount of terrigenous aerosols lifted by vehicles or by the wind from the roads and sidewalks that generally have a bad tarmac.

Fixed measurements were performed in the cities during the night stops and enabled the determination of LR profiles through a complete Raman inversion or a multi-layer constrained Klett inversion. Several events of biomass burning plumes were recorded during these nighttime observations, with LR values ranging from 63 to 107 sr and PDR values of from 1 to 4 %. Desert dust layers were also observed, with LR (PDR) values of 43 ± 14 sr (23 ± 2 %) for pure dust and 75 ± 9 sr (13 ± 3 %) for a mixed dust and biomass burning layer. The back-trajectory analysis identifies the dust source in the region of the Caspian and Aral Seas (south-western Kazakhstan), an area whose dust emissions had not been characterized so far. Moreover, dust layers were observed from Moscow to Omsk (37-73°E, ~2,300 km), demonstrating that the Caspian-Aral region can give birth to large dust events spreading over wide areas of Russia and lasting for several days. Such an event does not require special conditions but a regular anticyclone moving eastwards over northern Kazakhstan, meaning

such dust spreading could happen regularly and contribute significantly to the aerosol budget in southern Russia.

This ground-based mobile campaign provides a unique picture of summer aerosols in areas where observations are usually scarce. Although it is only a snapshot and no climatology, these observations hold more representativeness for two reasons: first, the lidar instrument involved in this campaign enabled the determination of two intensive properties of the particles (LR and PDR) that do not depend on aerosol amounts. And secondly, the comparison with a multi-annual average of MODIS Terra observations showed that the AOT values observed during the campaign are representative of the aerosol loads existing over Europe and Russia in the absence of exceptional fire events. Only the area where the dust event took place stands out from MODIS multi-annual average, however, it offered the opportunity to characterize the unstudied desert dust from the Caspian-Aral region.

Appendix A: details on the lidar ratio retrieval processes

Raman inversion. To differentiate the optical depth profile provided by the Raman channel, we use a low-pass derivative filter which kernel is based on the first derivative of a Gaussian curve (ter Haar Romeny et al., 1993) as it allows a much better rejection of high frequencies, i.e. short-scale fluctuations in the extinction profile, than the more commonly used Savitzky-Golay filters or sliding window linear fit (the difference is around 30 dB). To take into account the decrease of the signal-to-noise ratio (SNR) with increasing altitude, the filter width σ is increased following a saturating exponential function $\sigma(z) = a + b \cdot (1 - \exp(-z/1.5))$ with z the altitude above ground level (a.g.l.) in km. The effective vertical resolution of the retrieved extinction profile is defined as the inverse of the spatial cut-off frequency (i.e. the frequency at which the filter response reaches $1/e$ of its maximum amplitude). With $a = 3$ and $b = 7$ (our standard set of parameters), the effective vertical resolution tends towards 200 m at 5 km a.g.l., while the pair $a = 1$ and $b = 24$ (which we use in low SNR conditions) produces a coarser resolution profile (~500 m).

Single layer constrained Klett inversion. The Raman channel is used to determine the partial AOT between 300 m (complete overlap) and 700 m a.g.l. (range limit) which is then used to constrain the LR used in the Klett inversion. The principle is the same as described in Royer et al. (2011), except that the convergence is not dealt with using a dichotomy

algorithm. Indeed, due to the transmission by the upper layers, the partial AOT is not always a monotonic function of the LR. Instead, the extinction profile is inversed using 13 LR values distributed from 10 to 130 sr, a range covering LR values observed in the literature for the main types of aerosols (Table 1, Table 2 and Table 3). Then, the interval is narrowed between the two LR values that produce the best partial AOT and the process is repeated. After three iterations, the LR value giving the best agreement with the Raman constraint is chosen, the LR is known by 0.1 sr and the agreement is better than 10^{-3}, if a solution exists. According to the sensitivity study carried out by Royer et al. (2011), the main source of uncertainty on the LR value is the random detection processes. It leads to a relative error on the LR ranging between 4 and 18 % (16 to 100 %) during nighttime (daytime) for AOT values ranging from 0.1 to 0.5 and with a signal to noise ratio of 35 (10). For the lidar-derived AOT the relative uncertainty stands between 4 and 16 % (12 to 40 %) during nighttime (daytime) for the same SNR values.

Multi-layer constrained Klett inversion. When the Raman channel has a longer detection range than 700 m a.g.l. (during nighttime), the process described in the previous section can be applied over several successive layers. At first, the constraint zone is located just below the normalization zone, or just below the limit range of the Raman channel. The LR value giving the best agreement between the partial AOT from the Raman channel and from Klett's inversion is determined and attributed to this layer. Then, the constraint zone is translated downwards and the process is repeated until reaching the ground level. Layers where the aerosol load is too small (average extinction coefficient lower than 0.02 km^{-1}) are ignored and the LR from the layer located directly above them is kept. The constraint zone width is chosen between 200 to 900 m, depending on the aerosol load. The case studies that will be presented in Section 4 show that this method gives similar results as the derivative Raman inversion, with the advantage of producing a smoother LR profile (no fluctuations in the layers with a low aerosol load).

Appendix B: uncertainties on the depolarization

Apart from measurement noise, the sources of error on the retrieved Particulate Depolarization Ratio (PDR) are (*i*) the uncertainty on the lidar ratio, (*ii*) the uncertainty on the gain ratio and (*iii*) the error on the cross-talk between the total and perpendicular polarization channels. The impact of the former is estimated using the uncertainty on the lidar ratio when it is known (i.e. for case studies) or by varying LR by an arbitrary ± 10 sr as in Freudenthaler

et al. (2009), which corresponds to a 48-68 sr interval, for the systematic processing. The second and third terms are assessed by varying both the gain ratio (by its observed variability) and the coefficients of the separating plates (measured in the lab) by ± 5 %. When considering the average PDR in a layer, like in Section 4.1, the atmospheric variability (measured as the vertical standard deviation) in the layer is added as a fourth source of error. The contributions are then combined through a quadratic sum.

The error on PDR estimated by the process explained above is computed by a Monte-Carlo simulation of dummy lidar profiles with thin layers (scattering ratio between 1.02 and 1.2) in the noise conditions of each study (i.e. systematic processing, nighttime case study 50-minute average and 5-minute average).As an example, Figure B1 shows the results of this simulation conducted in the conditions of the Kazan case study (50-minute average after dusk), for a layer with a homogenous PDR of 1 or 5%, a scattering ratio from 1.02 to 1.2, and error on LR varying from 2 to 10 sr. The error on the gain ratio and on the coefficients of the polarization separation plates is fixed at 5% each. Note that because of the small number of average profiles and the remaining sunlight after dusk, the noise condition considered here represent a worst case for nighttime observations. We find that, given the chosen scattering ratio threshold of 1.05, the relative uncertainty on the PDR is largely constrained by the one on the lidar ratio for PDR values of 5% and above and below 4 km a.g.l.. Because of the error on the gain ratio, this relative uncertainty is always at least 7%. For very low PDR values, the absolute uncertainty mostly depends on noise conditions, but remains above 0.2%.

Acknowledgements

The authors would like to thank Dr Frederik Paulsen, Honorary Consul for the Russian Federation in the canton of Vaud, Switzerland, both for his financial support and for obtaining the permission to operate in Russia. The authors are also very grateful to Dr Alexander Ayurzhanaev from the Siberian Branch of the Russian Academy of Sciences, Laboratory of Physics of Atmospheric Processes, Ulan-Ude, for his vital help with the logistic of the journey while he was aboard the van. We also thank Yoann Chazette for his help during the trip. Finally, the authors thank Cyril Moulin, head of the Laboratoire des Sciences du Climat et de l'Environnement, for his support and assistance in the administrative part of the project.

References

Amiridis, V., Balis, D. S., Giannakaki, E., Stohl, A., Kazadzis, S., Koukouli, M. E. and Zanis, P.: Optical characteristics of biomass burning aerosols over Southeastern Europe determined from UV-Raman lidar measurements, Atmos. Chem. Phys., 9(7), 2431–2440, doi:10.5194/acp-9-2431-2009, 2009.

Amiridis, V., Balis, D. S., Kazadzis, S., Bais, A., Giannakaki, E., Papayannis, A. and Zerefos, C.: Four-year aerosol observations with a Raman lidar at Thessaloniki, Greece, in the framework of European Aerosol Research Lidar Network (EARLINET), J. Geophys. Res., 110, D21203, doi:10.1029/2005JD006190, 2005.

Ansmann, A., Engelmann, R., Althausen, D., Wandinger, U., Hu, M., Zhang, Y. and He, Q.: High aerosol load over the Pearl River Delta, China, observed with Raman lidar and Sun photometer, Geophys. Res. Lett., 32(13), 13815, doi:10.1029/2005GL023094, 2005.

Ansmann, A., Riebesell, M. and Weitkamp, C.: Measurement of atmospheric aerosol extinction profiles with a Raman lidar, Opt. Lett., 15(13), 746–748, doi:10.1364/OL.15.000746, 1990.

Ansmann, A., Tesche, M., Seifert, P., Groß, S., Freudenthaler, V., Apituley, A., Wilson, K. M., Serikov, I., Linné, H., Heinold, B., Hiebsch, A., Schnell, F., Schmidt, J., Mattis, I., Wandinger, U. and Wiegner, M.: Ash and fine-mode particle mass profiles from EARLINET-AERONET observations over central Europe after the eruptions of the Eyjafjallajökull volcano in 2010, J. Geophys. Res. Atmos., 116, doi:10.1029/2010JD015567, 2011.

Bates, T. S., Huebert, B. J., Gras, J. L., Griffiths, F. B. and Durkee, P. A.: International Global Atmospheric Chemistry (IGAC) Project's First Aerosol Characterization Experiment (ACE1): Overview, J. Geophys. Res., 103, 16297, doi:10.1029/97JD03741, 1998.

Burton, S. P., Ferrare, R. A., Hostetler, . A, Hair, J. W., Rogers, R. R., Obland, M. D., Butler, C. F., Cook, A. L., Harper, D. B. and Froyd, K. D.: Aerosol classification using airborne High Spectral Resolution Lidar measurements - methodology and examples, Atm. Meas. Tech., 5, 73–98, doi:10.5194/amt-5-73-2012, 2012.

Cattrall, C., Reagan, J., Thome, K. and Dubovik, O.: Variability of aerosol and spectral lidar and backscatter and extinction ratios of key aerosol types derived from selected Aerosol Robotic Network locations, J. Geophys. Res., 110, D10S11, doi:10.1029/2004JD005124, 2005.

Chazette, P., Dabas, A., Sanak, J., Lardier, M. and Royer, P.: French airborne lidar measurements for Eyjafjallajökull ash plume survey, Atmos. Chem. Phys., 12(15), 7059–7072, doi:10.5194/acp-12-7059-2012, 2012.

Chazette, P., Marnas, F. and Totems, J.: The mobile Water vapor Aerosol Raman LIdar and its implication in the frame of the HyMeX and ChArMEx programs: application to a dust transport process, Atm. Meas. Tech., 7, 1629–1647, doi:10.5194/amt-7-1629-2014, 2014.

Chazette, P., Randriamiarisoa, H., Sanak, J., Couvert, P. and Flamant, C.: Optical properties of urban aerosol from airborne and ground-based in situ measurements performed during the Etude et Simulation de la Qualité de l'air en Ile de France (ESQUIF) program, J. Geophys. Res., 110, 2206, doi:10.1029/2004JD004810, 2005.

Chazette, P., Raut, J.-C., Dulac, F., Berthier, S., Kim, S.-W., Royer, P., Sanak, J., Loaëc, S. and Grigaut-Desbrosses, H.: Simultaneous observations of lower tropospheric continental aerosols with a ground-based, an airborne, and the spaceborne CALIOP lidar system, J. Geophys. Res., 115, D00H31, doi:10.1029/2009JD012341, 2010.

Chazette, P., Sanak, J. and Dulac, F.: New approach for aerosol profiling with a lidar onboard an ultralight aircraft: application to the African Monsoon Multidisciplinary Analysis, Env. Sci. Tech., 41, 8335–8341, doi:10.1021/es070343y, 2007.

Deuzé, J. L., Bréon, F.-M., Devaux, C., Goloub, P., Herman, M., Lafrance, B., Maignan, F., Marchand, A., Nadal, F., Perry, G. and Tanré, D.: Remote sensing of aerosols over land surfaces from POLDER-ADEOS-1 polarized measurements, J. Geophys. Res., 106, 4913–4926, doi:10.1029/2000JD900364, 2001.

Franke, K., Ansmann, A., Müller, D., Althausen, A., Wagner, F. and Scheele, R.: One-year observations of particle lidar ratio over the tropical Indian Ocean with Raman lidar, Geophys. Res. Lett., 28(24), 4559–4562, doi:10.1029/2001GL013671, 2001.

Franke, K., Ansmann, A., Müller, D., Althausen, D., Venkataraman, C., Shekar Reddy, M., Wagner, F. and Scheele, R.: Optical properties of the Indo-Asian haze layer over the tropical Indian Ocean, J. Geophys. Res., 108(D2), 4059, doi:10.109/2002JD002473, 2003.

Freudenthaler, V., Esselborn, M., Wiegner, M., Heese, B., Tesche, M., Ansmann, A., Müller, D., Althausen, D., Wirth, M., Fix, A., Ehret, G., Knippertz, P., Toledano, C., Gasteiger, J., Garhammer, M. and Seefeldner, M.: Depolarization ratio profiling at several wavelengths in

pure Saharan dust during SAMUM 2006, Tellus, Ser. B Chem. Phys. Meteorol., 61, 165–179, doi:10.1111/j.1600-0889.2008.00396.x, 2009.

Giglio, L., Csiszar, I. and Justice, C. O.: Global distribution and seasonality of active fires as observed with the Terra and Aqua Moderate Resolution Imaging Spectroradiometer (MODIS) sensors, J. Geophys. Res., 111, 2016, doi:10.1029/2005JG000142, 2006.

Groß, S., Tesche, M., Freudenthaler, V., Toledano, C., Wiegner, M., Ansmann, A., Althausen, D. and Seefeldner, M.: Characterization of Saharan dust, marine aerosols and mixtures of biomass-burning aerosols and dust by means of multi-wavelength depolarization and Raman lidar measurements during SAMUM 2, Tellus, Ser. B Chem. Phys. Meteorol., 63, 706–724, doi:10.1111/j.1600-0889.2011.00556.x, 2011.

Ter Haar Romeny, B. M., Florack, L. M. J., Salden, A. H. and Viergever, M. A.: Higher order differential structure of images, in Information Processing in Medical Imaging, edited by H. H. Barrett and A. F. Gmitro, pp. 77–93, Springer, Berlin Heidelberg., 1993.

Heintzenberg, J., Birmili, W., Seifert, P., Panov, A., Chi, X. and Andreae, M.: Mapping the aerosol over Eurasia from the Zotino Tall Tower, Tellus B, 65, 20062, doi:10.3402/tellusb.v65i0.20062, 2013.

Holben, B. N., Eck, T. F., Slutsker, I., Tanré, D., Buis, J. P., Setzer, A., Vermote, E., Reagan, J. A., Kaufman, Y. J., Nakajima, T., Lavenu, F., Jankowiak, I. and Smirnov, A.: AERONET-A Federated Instrument Network and Data Archive for Aerosol Characterization, Rem. Sens. Env., 66(1), 1–16, doi:10.1016/S0034-4257(98)00031-5, 1998.

Huebert, B. J., Bates, T., Russell, P. B., Shi, G., Kim, Y. J., Kawamura, K., Carmichael, G. and Nakajima, T.: An overview of ACE-Asia: Strategies for quantifying the relationships between Asian aerosols and their climatic impacts, J. Geophys. Res., 108, 8633, doi:10.1029/2003JD003550, 2003.

IPCC: The Physical Science Basis. Contribution of Working Group I to the Fifth Assessment Report of the Intergovernmental Panel on Climate Change, edited by T. F. Stocker, D. Qin, G.-K. Plattner, M. Tignor, S. K. Allen, J. Boschung, A. Nauels, Y. Xia, V. Bex, and P. M. Midgley, Cambridge University Press, Cambridge, United Kingdom and New York, NY, USA., 2013.

King, M. D., Kaufman, Y. J., Menzel, W. P. and Tanré, D.: Remote sensing of cloud, aerosol, and water vapor properties from the moderate resolution imaging spectrometer (MODIS), IEEE T. Geosci. Remote, 30, 2–27, doi:10.1109/36.124212, 1992.

Klett, J. D.: Lidar inversion with variable backscatter/extinction ratios., Appl. Opt., 24, 1638–1643, doi:10.1364/AO.25.000833, 1985.

Law, K. S., Stohl, A., Quinn, P. K., Brock, C., Burkhart, J., Paris, J.-D., Ancellet, G., Singh, H. B., Roiger, A., Schlager, H., Dibb, J., Jacob, D. J., Arnold, S. R., Pelon, J. and Thomas, J. L.: Arctic Air Pollution: New Insights From POLARCAT-IPY, Bull. Am. Meteorol. Soc., in press [online] Available from: http://dx.doi.org/10.1175/BAMS-D-13-00017.1, 2014.

Lebel, T., Parker, D. J., Flamant, C., Bourlès, B., Marticorena, B., Mougin, E., Peugeot, C., Diedhiou, A., Haywood, J. M., Ngamini, J. B., Polcher, J., Redelsperger, J.-L. and Thorncroft, C. D.: The AMMA field campaigns: multiscale and multidisciplinary observations in the West African region, Q. J. R. Meteorol. Soc., 136, 8–33, doi:10.1002/qj.486, 2010.

Mamouri, R. E., Ansmann, A., Nisantzi, A., Kokkalis, P., Schwarz, A. and Hadjimitsis, D.: Low Arabian dust extinction-to-backscatter ratio, Geophys. Res. Lett., 40, 4762–4766, doi:10.1002/grl.50898, 2013.

Mattis, I., Ansmann, A., Müller, D., Wandinger, U. and Althausen, D.: Multiyear aerosol observations with dual-wavelength Raman lidar in the framework of EARLINET, J. Geophys. Res., 109(D18), 13203, doi:10.1029/2004JD004600, 2004.

Molina, L. T., Madronich, S., Gaffney, J. S., Apel, E., De Foy, B., Fast, J., Ferrare, R., Herndon, S., Jimenez, J. L., Lamb, B., Osornio-Vargas, A. R., Russell, P., Schauer, J. J., Stevens, P. S., Volkamer, R. and Zavala, M.: An overview of the MILAGRO 2006 Campaign: Mexico City emissions and their transport and transformation, Atm. Chem. Phys., 10(18), 8697–8760, doi:10.5194/acp-10-8697-2010, 2010.

Müller, D., Ansmann, A., Mattis, I., Tesche, M., Wandinger, U., Althausen, D. and Pisani, G.: Aerosol-type-dependent lidar ratios observed with Raman lidar, J. Geophys. Res., 112, 16202, doi:10.1029/2006JD008292, 2007.

Müller, D., Lee, K.-H., Gasteiger, J., Tesche, M., Weinzierl, B., Kandler, K., Müller, T., Toledano, C., Otto, S., Althausen, D. and Ansmann, A.: Comparison of optical and microphysical properties of pure Saharan mineral dust observed with AERONET Sun

photometer, Raman lidar, and in situ instruments during SAMUM 2006, J. Geophys. Res., 117, 7211, doi:10.1029/2011JD016825, 2012.

Müller, D., Mattis, I., Wandinger, U., Ansmann, A., Althausen, D. and Stohl, A.: Raman lidar observations of aged Siberian and Canadian forest fire smoke in the free troposphere over Germany in 2003: Microphysical particle characterization, J. Geophys. Res., 110, 17201, doi:10.1029/2004JD005756, 2005.

Murayama, T., Müller, D., Wada, K., Shimizu, A., Sekiguchi, M. and Tsukamoto, T.: Characterization of Asian dust and Siberian smoke with multi-wavelength Raman lidar over Tokyo, Japan in spring 2003, Geophys. Res. Lett., 31, 23103, doi:10.1029/2004GL021105, 2004.

Nicolae, D., Nemuc, A., Müller, D., Talianu, C., Vasilescu, J., Belegante, L. and Kolgotin, A.: Characterization of fresh and aged biomass burning events using multiwavelength Raman lidar and mass spectrometry, J. Geophys. Res., 118, 2956–2965, doi:10.1002/jgrd.50324, 2013.

Nisantzi, A., Mamouri, R. E., Ansmann, A. and Hadjimitsis, D.: Injection of mineral dust into the free troposphere during fire events observed with polarization lidar at Limassol, Cyprus, Atm. Chem. Phys., 14(22), 12155–12165, doi:10.5194/acp-14-12155-2014, 2014.

Panchenko, M. V, Zhuravleva, T. B., Terpugova, S. A., Polkin, V. V and Kozlov, V. S.: An empirical model of optical and radiative characteristics of the tropospheric aerosol over West Siberia in summer, Atm. Meas. Tech., 5(7), 1513–1527, doi:10.5194/amt-5-1513-2012, 2012.

Pappalardo, G., Amodeo, A., Apituley, A., Comeron, A., Freudenthaler, V., Linné, H., Ansmann, A., Bösenberg, J., D'Amico, G., Mattis, I., Mona, L., Wandinger, U., Amiridis, V., Alados-Arboledas, L., Nicolae, D. and Wiegner, M.: EARLINET: towards an advanced sustainable European aerosol lidar network, Atmos. Meas. Tech., 7(8), 2389–2409, doi:10.5194/amt-7-2389-2014, 2014.

Paris, J.-D., Ciais, P., Nédélec, P., Stohl, A., Belan, B. D., Arshinov, M. Y., Carouge, C., Golitsyn, G. S. and Granberg, I. G.: New Insights on the Chemical Composition of the Siberian Air Shed from the YAK-AEROSIB Aircraft Campaigns, B. Am. Meteorol. Soc., 91, 625–641, doi:10.1175/2009BAMS2663.1, 2010.

Raes, F., Bates, T., McGovern, F. and Van Liedekerke, M.: The 2nd Aerosol Characterization Experiment (ACE2): general overview and main results, Tellus B, 52, 111, doi:10.1034/j.1600-0889.2000.00124.x, 2000.

Ramanathan, V., Crutzen, P. J., Lelieveld, J., Mitra, A. P., Althausen, D., Anderson, J., Andreae, M. O., Cantrell, W., Cass, G. R., Chung, C. E., Clarke, A. D., Coakley, J. A., Collins, W. D., Conant, W. C., Dulac, F., Heintzenberg, J., Heymsfield, A. J., Holben, B., Howell, S., Hudson, J., Jayaraman, A., Kiehl, J. T., Krishnamurti, T. N., Lubin, D., McFarquhar, G., Novakov, T., Ogren, J. A., Podgorny, I. A., Prather, K., Priestley, K., Prospero, J. M., Quinn, P. K., Rajeev, K., Rasch, P., Rupert, S., Sadourny, R., Satheesh, S. K., Shaw, G. E., Sheridan, P. and Valero, F. P. J.: Indian Ocean Experiment: An integrated analysis of the climate forcing and effects of the great Indo-Asian haze, J. Geophys. Res., 106(D22), 28371–28398, doi:10.1029/2001JD900133, 2001.

Raut, J.-C. and Chazette, P.: Retrieval of aerosol complex refractive index from a synergy between lidar, sunphotometer and in situ measurements during LISAIR experiment, Atmos. Chem. Phys., 7, 2797–2815, doi:10.5194/acp-9-8617-2009, 2007.

Royer, P., Chazette, P., Lardier, M. and Sauvage, L.: Aerosol content survey by mini N2-Raman lidar: Application to local and long-range transport aerosols, Atm. Env., 45, 7487–7495, doi:10.1016/j.atmosenv.2010.11.001, 2011.

Royer, P., Raut, J.-C., Ajello, G., Berthier, S. and Chazette, P.: Synergy between CALIOP and MODIS instruments for aerosol monitoring: application to the Po Valley, Atm. Meas. Tech., 3, 893–907, doi:10.5194/amt-3-893-2010, 2010.

Salomonson, V. V, Magner, T., Barnes, W., Montgomery, H. and Ostrow, H.: Moderate Resolution Imaging Spectrometer - A progress report (April 1989), in Quantitative Remote Sensing: An Economic Tool for the Nineties, Proceedings of IGARSS ’89 and of the 12th Canadian Symposium on Remote Sensing, pp. 2917–2921, IEEE, New York, Vancouver, Canada., 1989.

Schuster, G. L., Vaughan, M., MacDonnell, D., Su, W., Winker, D., Dubovik, O., Lapyonok, T. and Trepte, C.: Comparison of CALIPSO aerosol optical depth retrievals to AERONET measurements, and a climatology for the lidar ratio of dust, Atm. Chem. Phys., 12, 7431–7452, doi:10.5194/acp-12-7431-2012, 2012.

Tesche, M., Ansmann, A., Müller, D., Althausen, D., Engelmann, R., Hu, M. and Zhang, Y.: Particle backscatter, extinction, and lidar ratio profiling with Raman lidar in south and north China, Appl. Opt., 46(25), 6302–6308, doi:10.1364/AO.46.006302, 2007.

Tesche, M., Groß, S., Ansmann, A., Müller, D., Althausen, D., Freudenthaler, V. and Esselborn, M.: Profiling of Saharan dust and biomass-burning smoke with multiwavelength polarization Raman lidar at Cape Verde, Tellus B, 63, 649–676, doi:10.1111/j.1600-0889.2011.00548.x, 2011.

Vautard, R., Menut, L., Beekmann, M., Chazette, P., Flamant, P. H., Gombert, D., Guédalia, D., Kley, D., Lefebvre, M.-P., Martin, D., Mégie, G., Perros, P. and Toupance, G.: A synthesis of the Air Pollution Over the Paris Region (ESQUIF) field campaign, J. Geophys. Res., 108, 8558, doi:10.1029/2003JD003380, 2003.

Welton, E. J., Campbell, J. R., Spinhirne, J. D. and Scott, V. S.: Global monitoring of clouds and aerosols using a network of micro-pulse lidar systems, in Lidar Remote Sensing for Industry and Environmental Monitoring, in Proc. SPIE 4153, Lidar Remote Sensing for Industry and Environment Monitoring, edited by U. N. Singh, T. Itabe, and N. Sugimoto, pp. 151–158, Sendai, Japan., 2001.

Winker, D. M., Pelon, J. R. and McCormick, M. P.: The CALIPSO mission: spaceborne lidar for observation of aerosols and clouds, in Proc. SPIE 4893, Lidar Remote Sensing for Industry and Environment Monitoring III, edited by U. N. Singh, T. Itabe, and Z. Liu, pp. 1–11, Hangzhou, China., 2003.

Tables

Table 1. Values of the extinction-to-backscatter ratio (also called lidar ratio or LR) and Particle Depolarization Ratio (PDR) reported in the literature and observed in this study for desert dust aerosols, pure or mixed with biomass burning or pollution. For Burton et al. (2012), values are the 25-75th (5-95th) percentiles respectively.

Aerosol type	Site, campaign	Instrument, inversion method	λ (nm)	LR (sr)	PDR (%)	Reference
Pure dust	AERONET network	AERONET Sunphotometers	550	42 ± 4	-	Cattrall et al. (2005)
	North America, multi campaign	High spectral resolution lidar (HSRL)	532	44 – 51 (41 – 57)	31 – 33 (30 – 35)	Burton et al. (2012)
	Morocco & Cape Verde, SAMUM	N_2 Raman lidar	**355**	58 ± 7	25 ± 3	Groß et al. (2011) Müller et al. (2012)
	Thessaloniki (Greece) (Western Saharan dust)	N_2 Raman lidar	**355**	57 ± 29	-	Amiridis et al. (2005)
	Maldives Islands, INODEX (Saudi Arabian dust)	N_2 Raman lidar	**355**	38 ± 5	-	Müller et al. (2007)
	Beijing (China) (Gobi desert dust)	N_2 Raman lidar	532	35 ± 5	-	Müller et al. (2007)
	Tokyo (Japan)	N_2 Raman lidar	**355**	49 ± 9	~20	Murayama et al. (2004)
	Niamey (Niger)	N_2 Raman lidar	**355**	~50	-	Chazette et al. (2007)
	Sahel, Middle East, India	CALIOP / AERONET synergy	532	50, 39, 44	-	Schuster et al. (2012)
	Cyprus (Syrian dust)	N_2 Raman lidar	532	34 – 39	28 – 35	Mamouri et al. (2013)
Dusty mix	North America, multi campaign	HSRL	532	30 – 42 (15 – 63)	13 – 20 (10 – 28)	Burton et al. (2012)
	Mor. / C. Verde, SAMUM	N_2 Raman lidar	**355**	75 ± 9	18 ± 3	Groß et al. (2011) Müller et al. (2012)
	Niamey (Niger)	N_2 Raman lidar	**355**	~67	-	Chazette et al. (2007)
	Balearic islands, HyMeX	N_2 Raman lidar	**355**	47 – 63	16 – 19	Chazette et al. (2014)
Pure dust	Kazan, lower sub-layer	Multi-layer Raman constr.	**355**	43 ± 14	23 ± 2	*This study*
Dusty mix	Kazan, upper sub-layer			75 ± 9	13 ± 3	
Pure dust?	Omsk	Full Raman inversion		50 ± 13	17 ± 2	

Table 2. Same as Table 1 but for biomass burning aerosols, either freshly emitted or aged. When the Backscatter to Extinction Ratio (BER) and the Particle Depolarization Ratio (PDR) have been retrieved at different wavelengths, the two values of wavelength are given.

Aerosol type	Site, campaign	Instrument, inversion method	λ (nm)	LR (sr)	PDR (%)	Reference
Fresh smoke	North America, multi campaign	High spectral resolution lidar	532	34 – 46 (24 – 54)	3 – 5 (2 – 8)	Burton et al. (2012)
	Bucharest, EARLINET	N_2 Raman lidar	**355**	73 ± 12	-	Nicolae et al. (2013)
Aged smoke	AERONET network	Sun-photometer	550	60 ± 8	-	Cattrall et al. (2005)
	North America, multi campaign	High spectral resolution lidar	532	55 – 72 (46 – 86)	4 – 9 (2 – 15)	Burton et al. (2012)
	Tokyo (Siberian smoke)	N_2 Raman lidar	**355**	~40	5 – 8	Murayama et al. (2004)
	Leipzig, EARLINET	N_2 Raman lidar	**355** - 532	46 ± 13	<5	Müller et al. (2005)
	Thessaloniki (Greece) (from Russia, Ukraine)	N_2 Raman lidar	**355**	39 – 94	-	Amiridis et al. (2009)
	Morocco / Cape Verde, SAMUM	N_2 Raman lidar	**355** - 532	87 ± 17	5 ± 2	Tesche et al. (2011)
	Bucharest, EARLINET	N_2 Raman lidar	**355**	32 – 48	-	Nicolae et al. (2013)
Aged smoke	Kazan	Multi-layer Raman constr.	**355**	107 ± 14	4 ± 2	*This study*
	Ishim	Full Raman inversion		65 ± 6	3 ± 1	
	Omsk	Full Raman inversion		76 ± 10	4 ± 2	
	Nizhneudinsk	Full Raman inversion		63 ± 15	~1	

Table 3. Same as Table 1 and Table 2 but for pollution aerosols.

Site, campaign	Instrument, inversion method	λ (nm)	LR (sr)	PDR (%)	Reference
AERONET network	Sun-photometer	550	71 ± 10	-	Cattrall et al. (2005)
North America, multi campaign	High spectral resolution lidar	532	52 – 69 (42 – 80)	3 – 8 (2 – 11)	Burton et al. (2012)
Central Europe, EARLINET	N_2 Raman lidar	**355** - 532	58 ± 12	<5	Mattis et al. (2004) Müller et al. (2007)
Paris, ESQUIF	Lidar / sun-phot. synergy	532	59 – 77	-	Chazette et al. (2005)
Paris, LISAIR	N_2 Raman lidar	**355**	83 ± 22	-	Raut and Chazette (2007)
Paris	N_2 Raman lidar	**355**	85 ± 18	-	Royer et al. (2011)
Po Valley	CALIOP / MODIS synergy	532	83 ± 25	-	Royer et al. (2010)
North India South India (INDOEX) South-East Asia	N_2 Raman lidar	532	65 ± 16 37 ± 10 51 ± 20	-	Franke et al. (2001) Franke et al. (2003)
Pearl River delta (China)	N_2 Raman lidar	532	47 ± 6	-	Ansmann et al. (2005)
Beijing (China)	N_2 Raman lidar	532	38 ± 7	-	Tesche et al. (2007)
Omsk (residual layer, after sunset / middle of night)	Full Raman inversion	**355**	67 ± 12 92 ± 18	4 ± 1 3 ± 1	*This study*

Figures

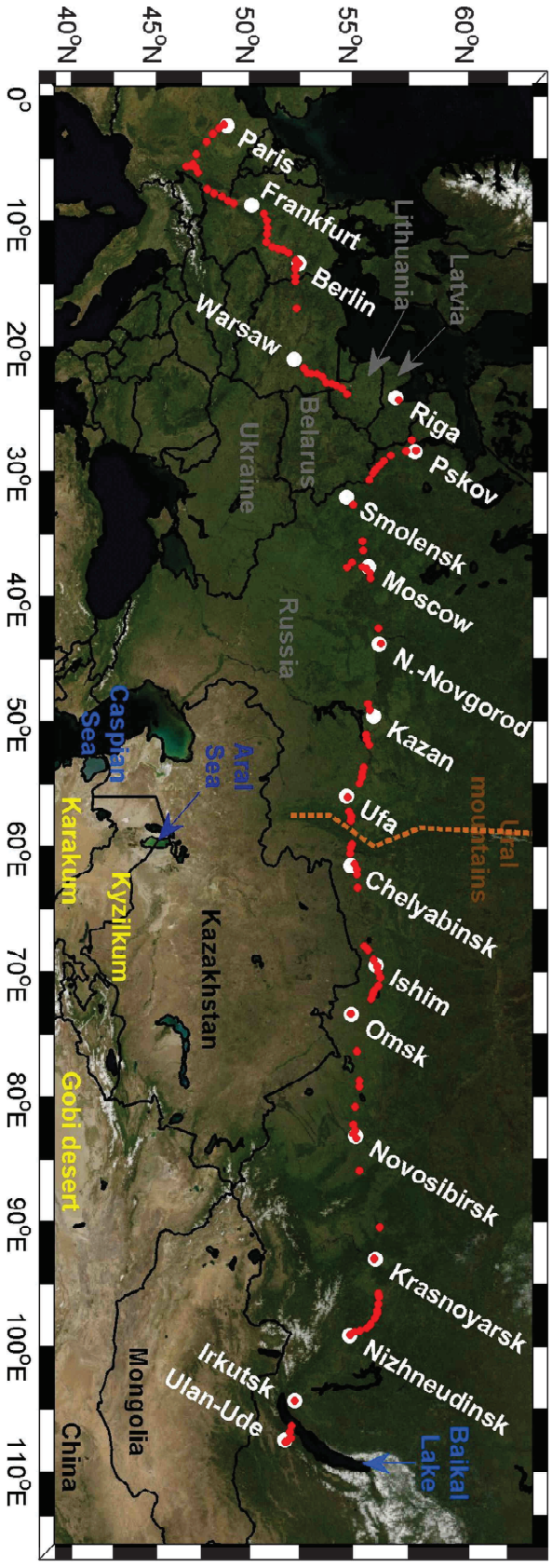
40°N
45°N
50°N
55°N
60°N
0°
10°E
20°E
30°E
40°E
50°E
60°E
70°E
80°E
90°E
100°E
110°E
Paris
Frankfurt
Berlin
Warsaw
Riga
Pskov
Smolensk
Moscow
N.-Novgorod
Kazan
Ufa
Chelyabinsk
Ishim
Omsk
Novosibirsk
Krasnoyarsk
Nizhneudinsk
Irkutsk
Ulan-Ude
Lithuania
Latvia
Belarus
Ukraine
Russia
Ural mountains
Caspian Sea
Aral Sea
Karakum
Kyzylkum
Kazakhstan
Gobi desert
Mongolia
China
Baikal Lake

1 Figure 1. Itinerary of the campaign plotted over MODIS true reflectance image. White and
2 red dots show respectively the main cities or night stops of the van, and the location of lidar
3 measurements.
4

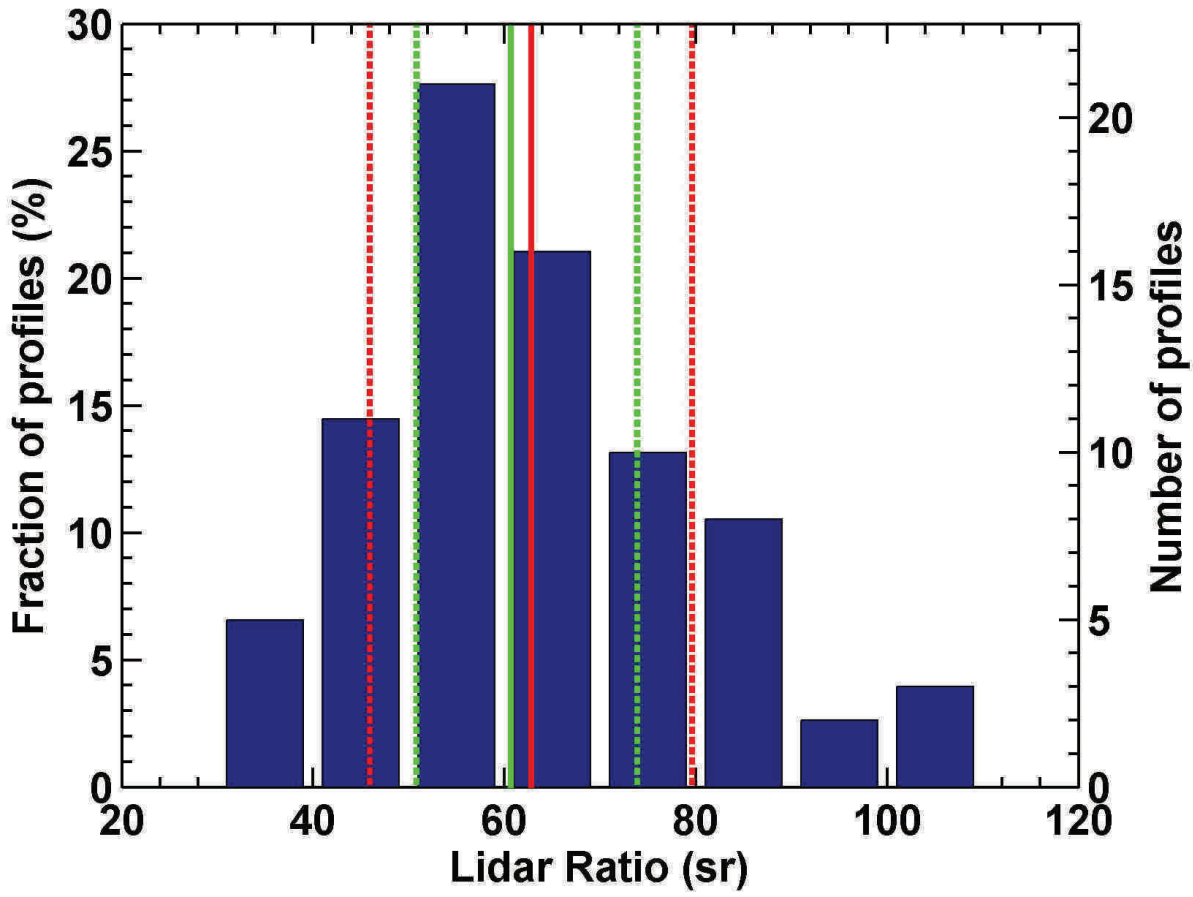

Figure 2. Distribution of the Lidar Ratio (LR) values obtained by constraining Klett's inversion with the partial aerosol optical thickness provided by the N_2-Raman channel between 0.3 and 0.7 km above ground level. The only profiles included are the 76 30-minute average profiles for which the agreement was better than 10^{-3} (and this for all the 200 profiles generated by the Monte-Carlo algorithm). Profiles from Istomino village (Lake Baikal shore) have also been removed. The red (resp. green) lines represent the LR average value and 1-σ standard deviation (resp. the median and quartiles).

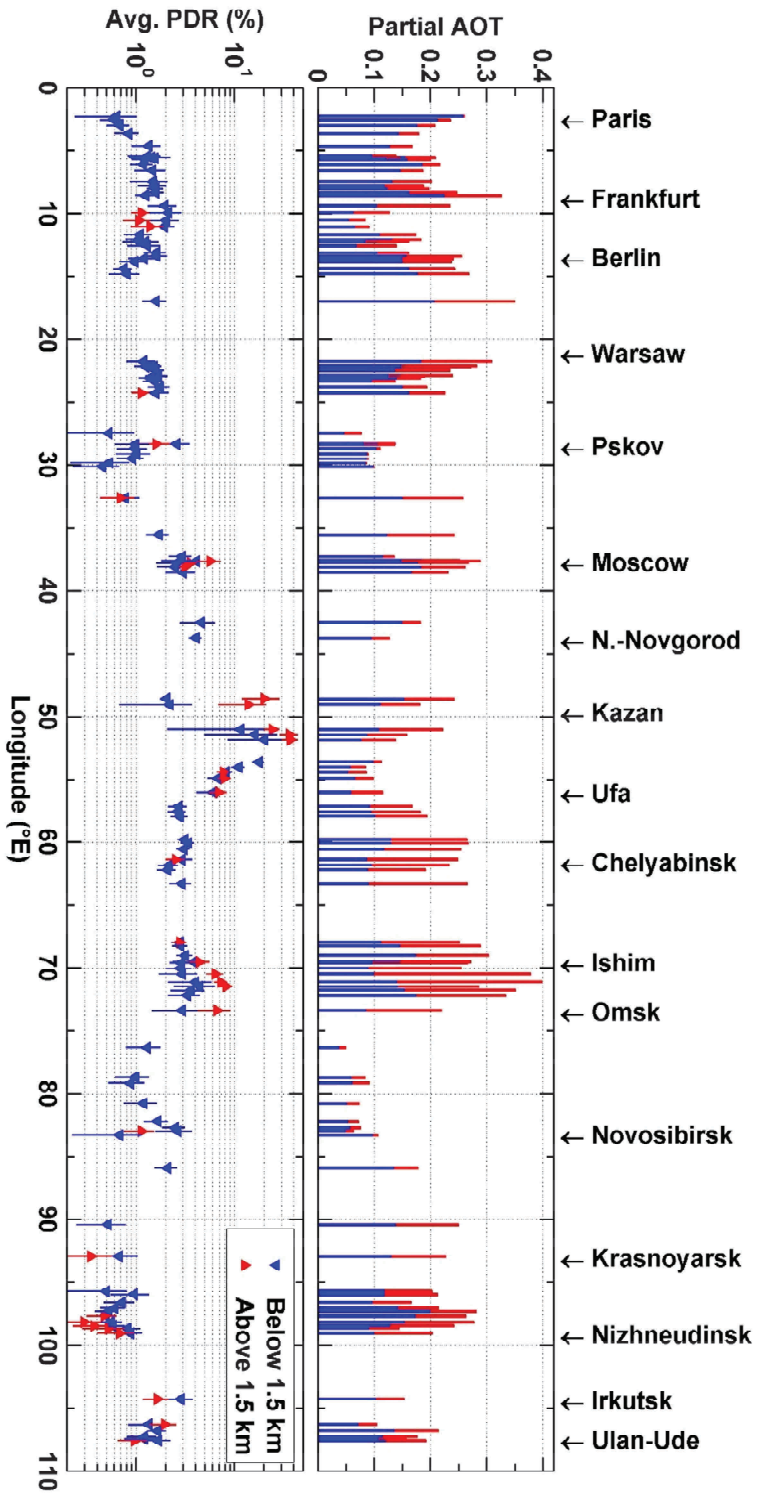

Figure 3. Partial Aerosol Optical Thickness (AOT, top) and average Particle Depolarization Ratio (PDR, bottom) along the route, computed below (in blue) and above (in red) 1500 m a.g.l. All values are inverted from the 30-minute average profiles using Klett's inversion with a fixed lidar ratio of 58 sr. The average PDR is computed only when the scattering ratio is greater than 1.05.

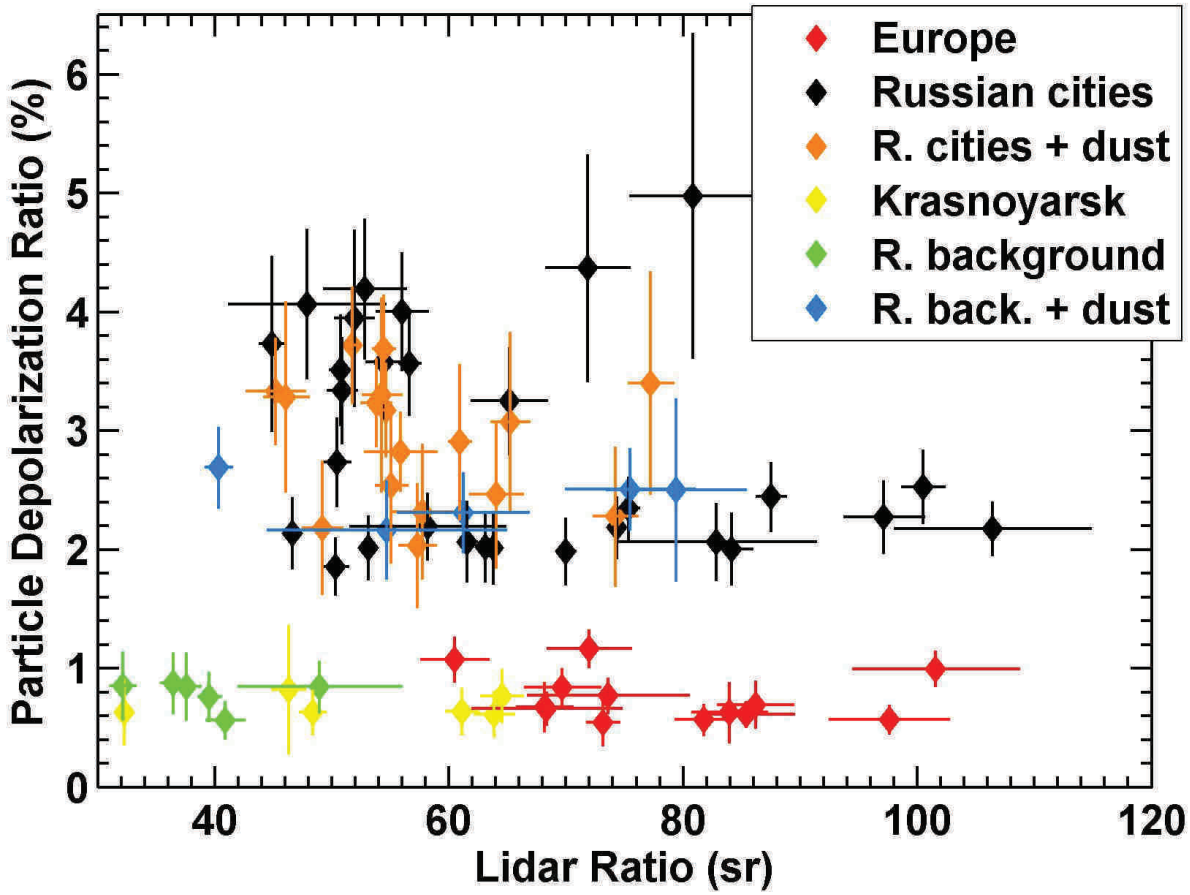

Figure 4. Scatter plot of the Particle Depolarization Ratio (PDR) *vs* Lidar Ratio (LR) values retrieved in the constraint zone (300-700 m averages) for the 76 convergent 30-minute average profiles from Figure 2. Profiles are sorted into 6 types of atmospheric and geographic conditions.

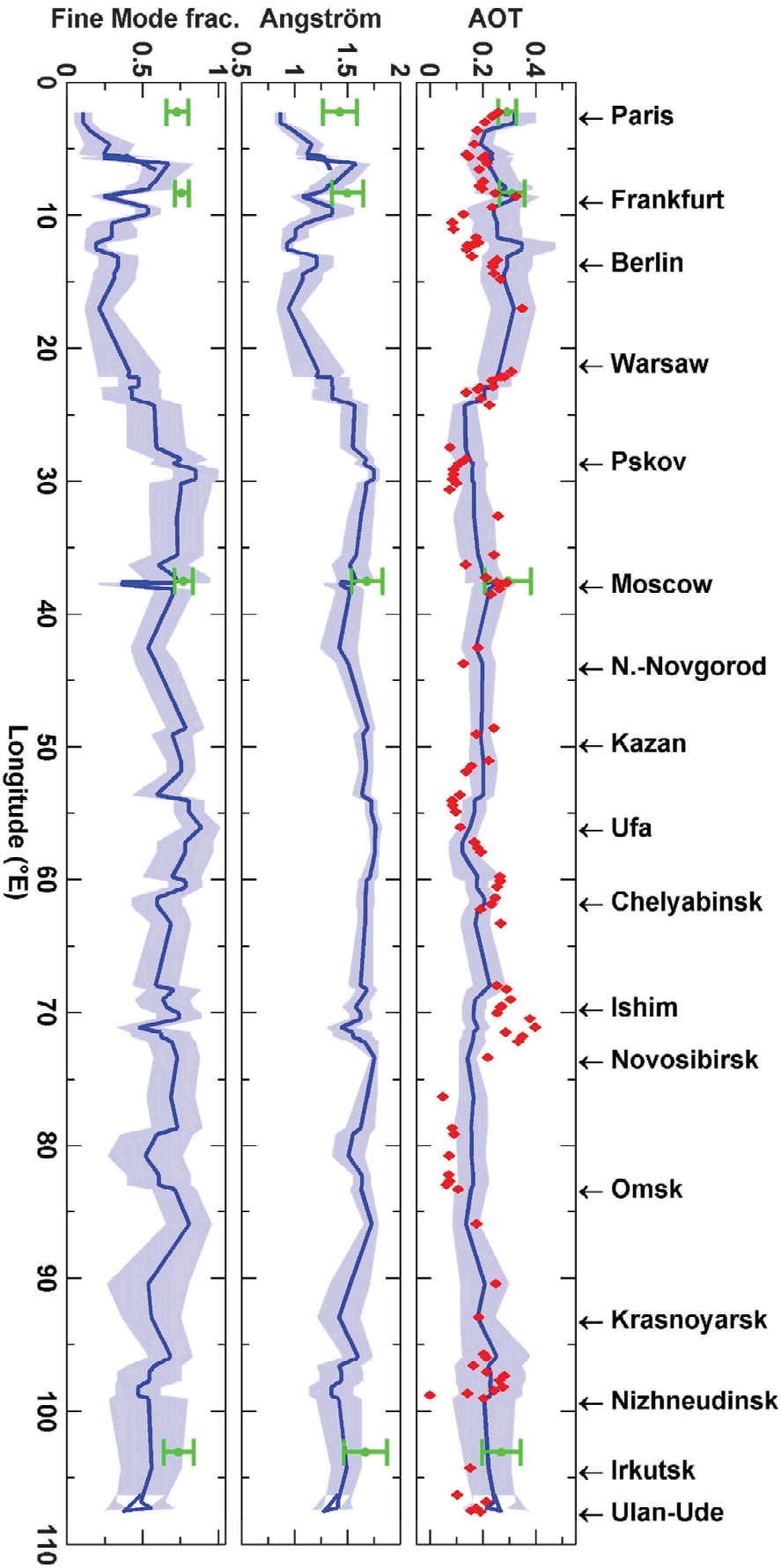
Fine Mode frac.
Angström
AOT
0
0.5
1
0.5
1
1.5
2
0
0.2
0.4
Longitude (°E)
0
10
20
30
40
50
60
70
80
90
100
110
← Paris
← Frankfurt
← Berlin
← Warsaw
← Pskov
← Moscow
← N.-Novgorod
← Kazan
← Ufa
← Chelyabinsk
← Ishim
← Novosibirsk
← Omsk
← Krasnoyarsk
← Nizhneudinsk
← Irkutsk
← Ulan-Ude

1

Figure 5. (top) Aerosol Optical Thickness (AOT) at 355 nm from the lidar (red), from MODIS Terra (blue) and from the AERONET stations along the transect (green). (middle) Ångström coefficients from MODIS Terra (470- 660 nm) and from AERONET (440-675 nm). (bottom) AOT small mode fraction from MODIS Terra (550 nm) and from AERONET (500 nm). For MODIS (MOD08_M3 product), the 1°×1° pixels including the van position were extracted and the months of June from years 2000 to 2013 (except years 2001, 2003 and 2012 due to intense fire events) were used to compute MODIS average and standard deviation (blue line and shading). For AERONET, only data since 2006 were used since only Palaiseau (2.5°E) has data prior to this year.

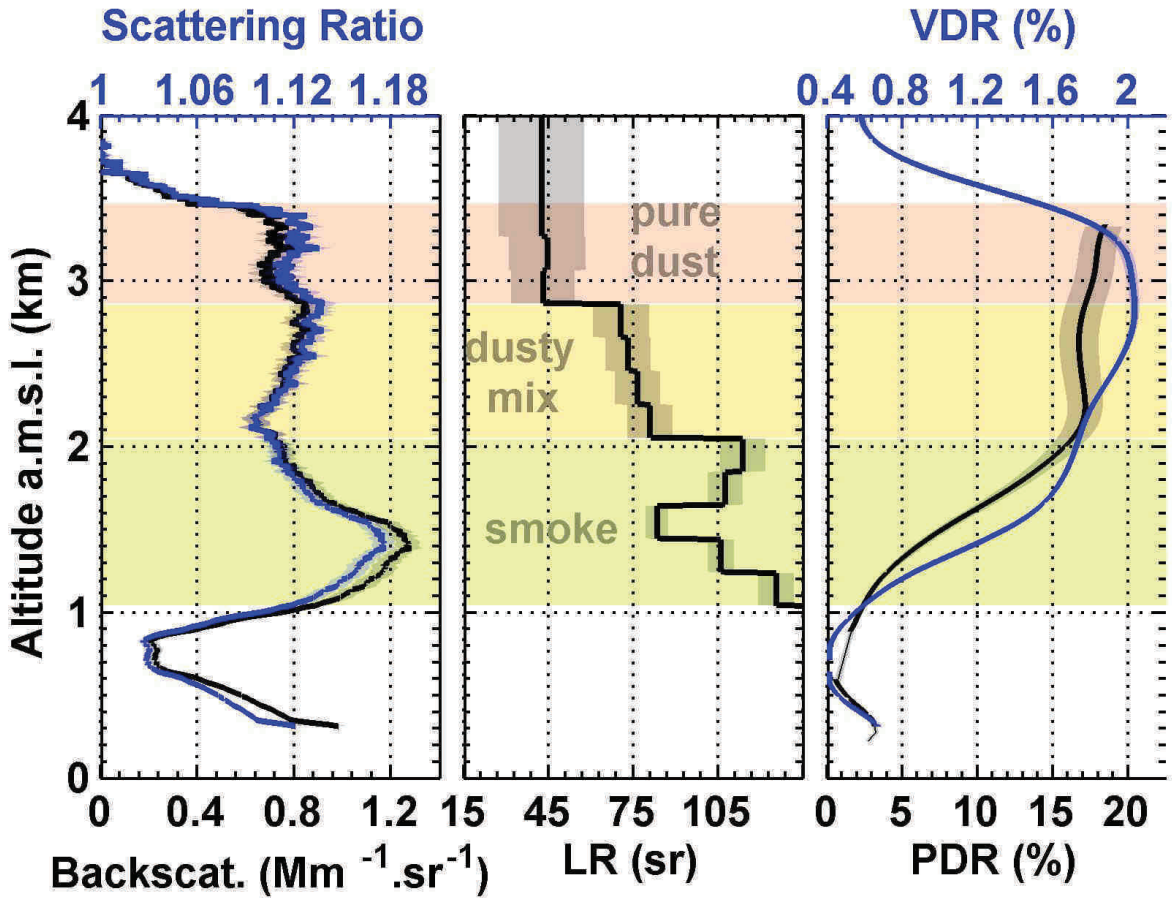

Figure 6. Vertical profiles of aerosol backscatter and Lidar Ratio (LR) determined from the 55-minute average profile on June 18th 2013, using either the low-pass derivative filter inversion (blue) or the constrained Klett procedure on a sliding 200 m window (red). Shaded areas represent the uncertainties from the Monte-Carlo process. For these mobile observations, the altitude is above mean sea level (a.m.s.l.); the ground average altitude was around 0.1 km a.m.s.l.

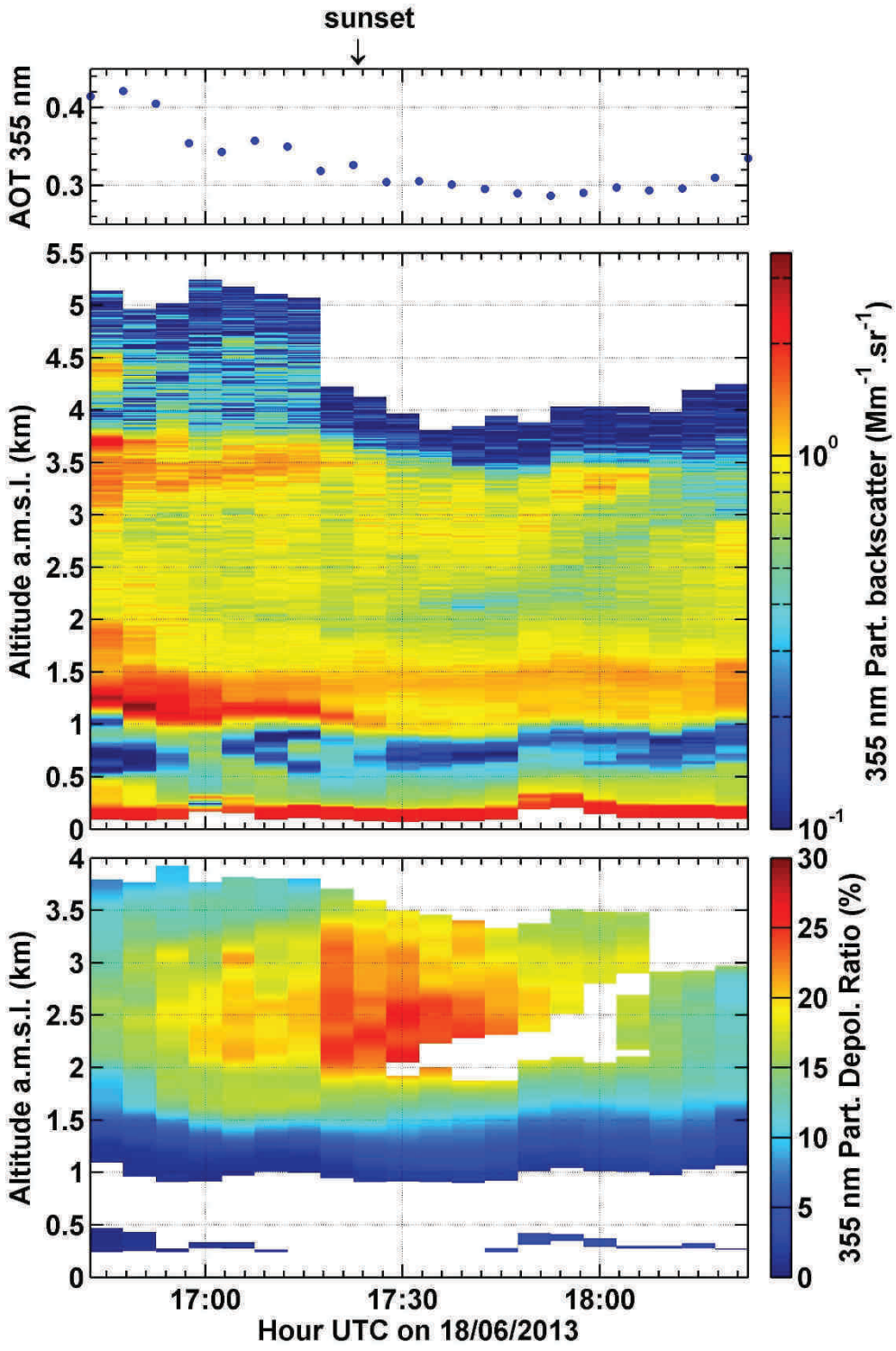

Figure 7. Aerosol Optical Thickness (AOT, top), backscatter (middle) and Particle Depolarization Ratio (PDR, bottom) observed West of Kazan on June 18th 2013 twilight as a function of UTC time and altitude above mean sea level (a.m.s.l.). Retrieval was made using a Klett inversion with the backscatter to extinction ratio profile from the sliding-window constrained Klett procedure (Figure 6, middle panel).

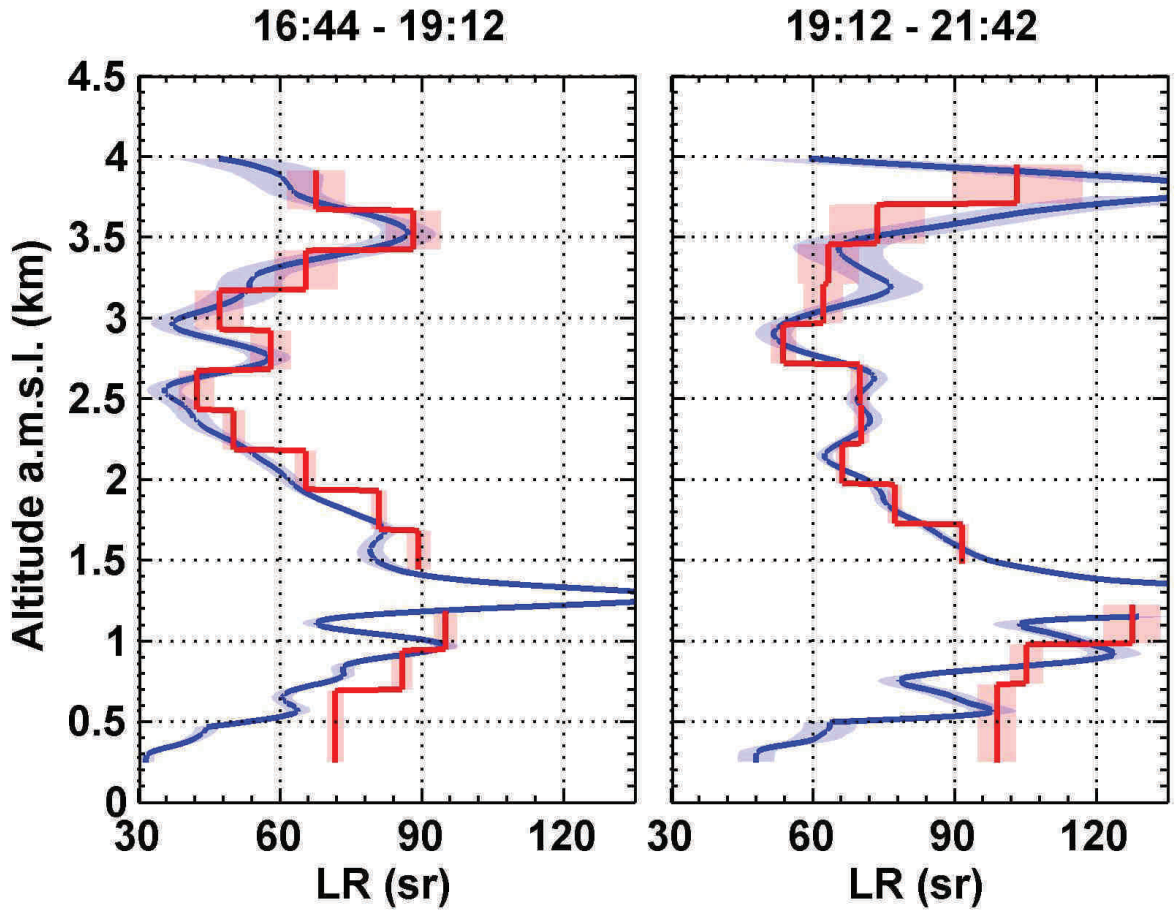

Figure 8. Profiles of Lidar Ratio (LR) retrieved above Omsk city on June 22nd 2013 from two different processes: (red) profiles from the sliding-window constrained Klett process, (blue) profiles from the low-pass derivative filter inversion (Raman inversion). Shaded areas represent the uncertainties from the Monte-Carlo process.

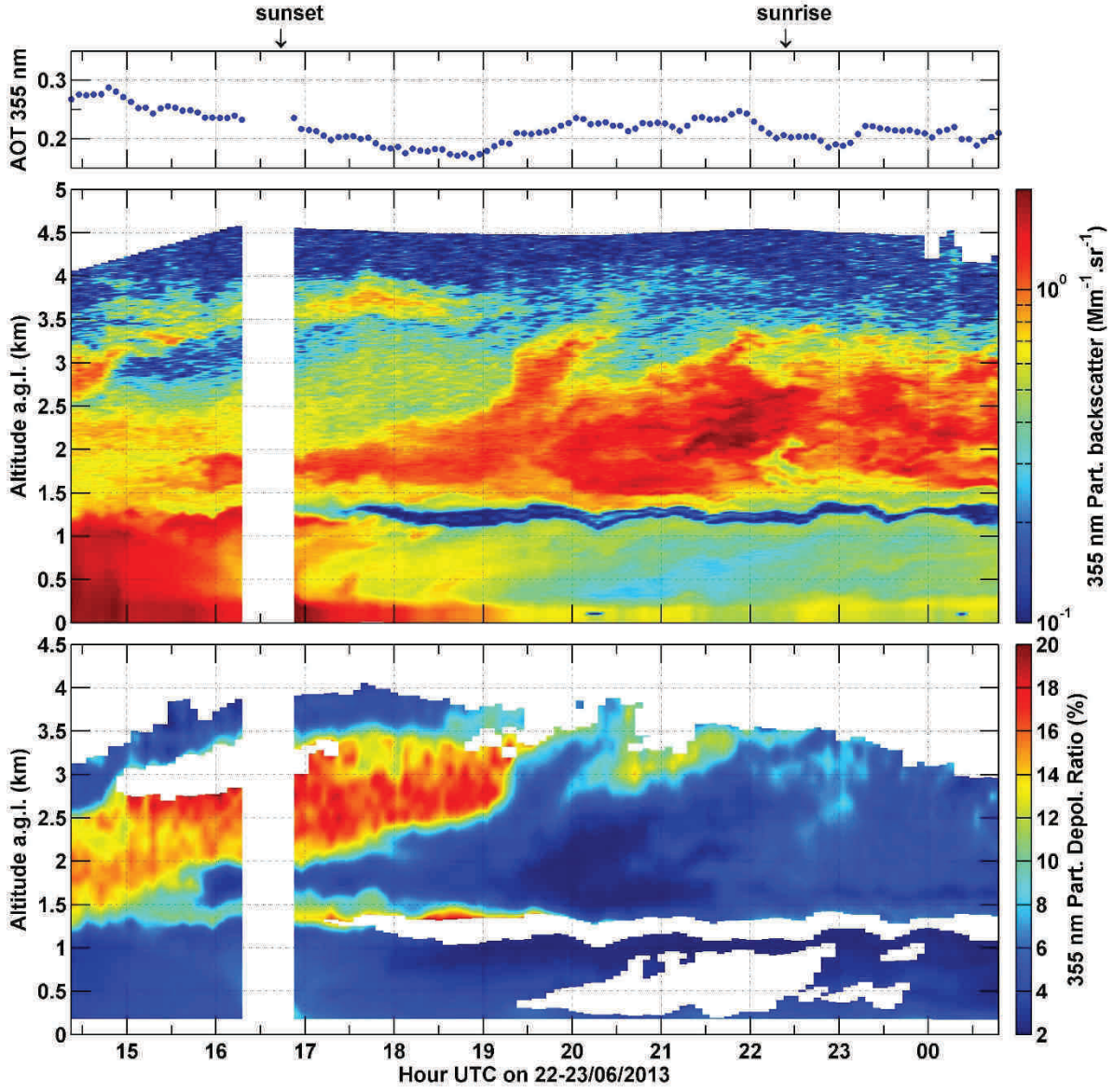

Figure 9. Aerosol Optical Thickness (AOT, top), backscatter (middle) and Particle Depolarization Ratio (bottom) retrieved above Omsk during the night from June 22nd to 23rd 2013 as a function of UTC time and altitude above ground level (a.g.l.). Retrieval was made using a Klett inversion with the lidar ratio profiles from Figure 8.

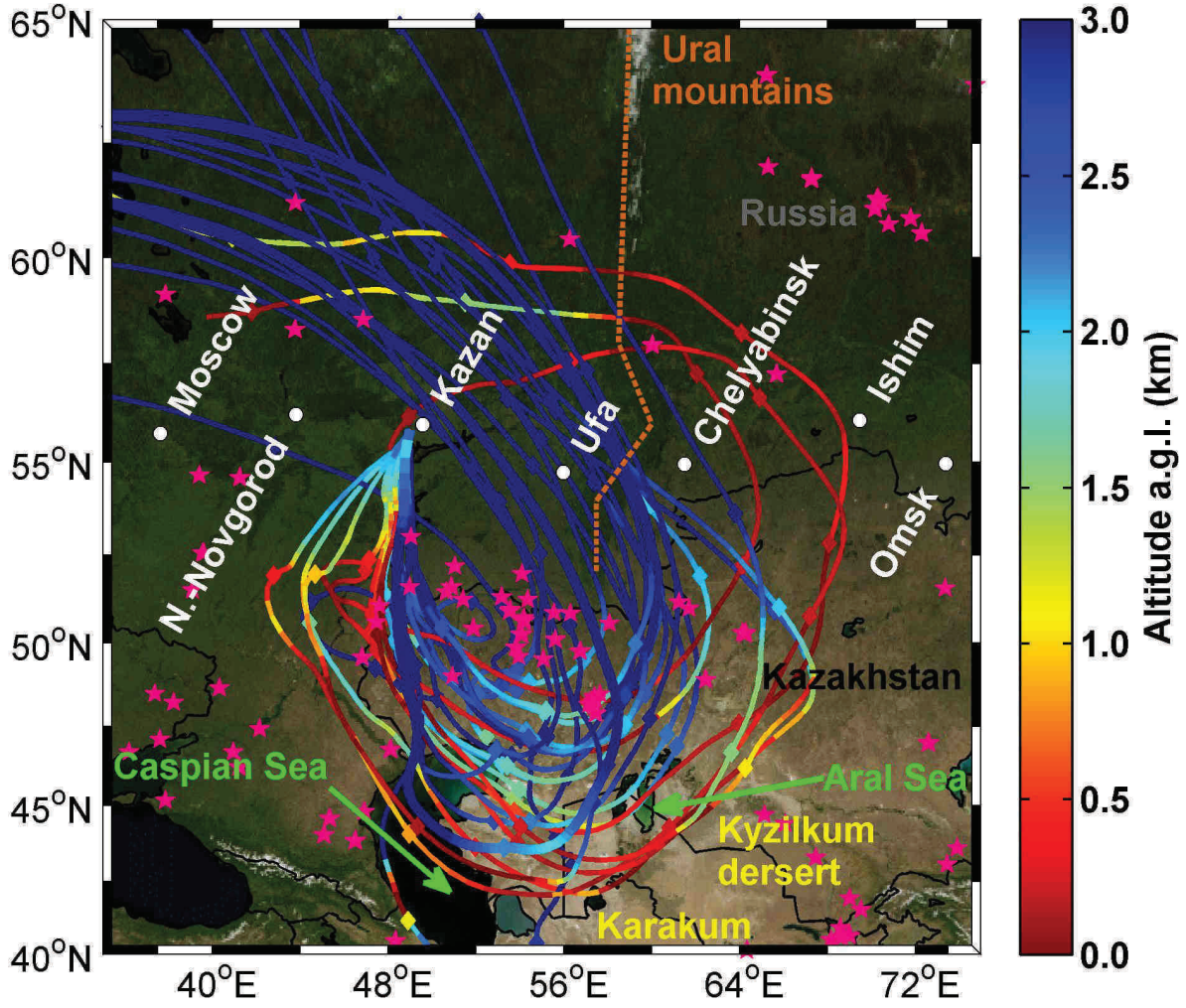

Figure 10. Seven-day back-trajectories ending in the dust layer observed west of Kazan city on June 18th 2013, computed using HYSPLIT Lagrangian model in single (bold line) and ensemble mode (thin lines). Trajectories are colored following the altitude above ground level (a.g.l.): red parts correspond to ground contact. Ticks are spaced by 24 hours. Pink stars represent MODIS fire hot-spots detected during the trajectories time period.

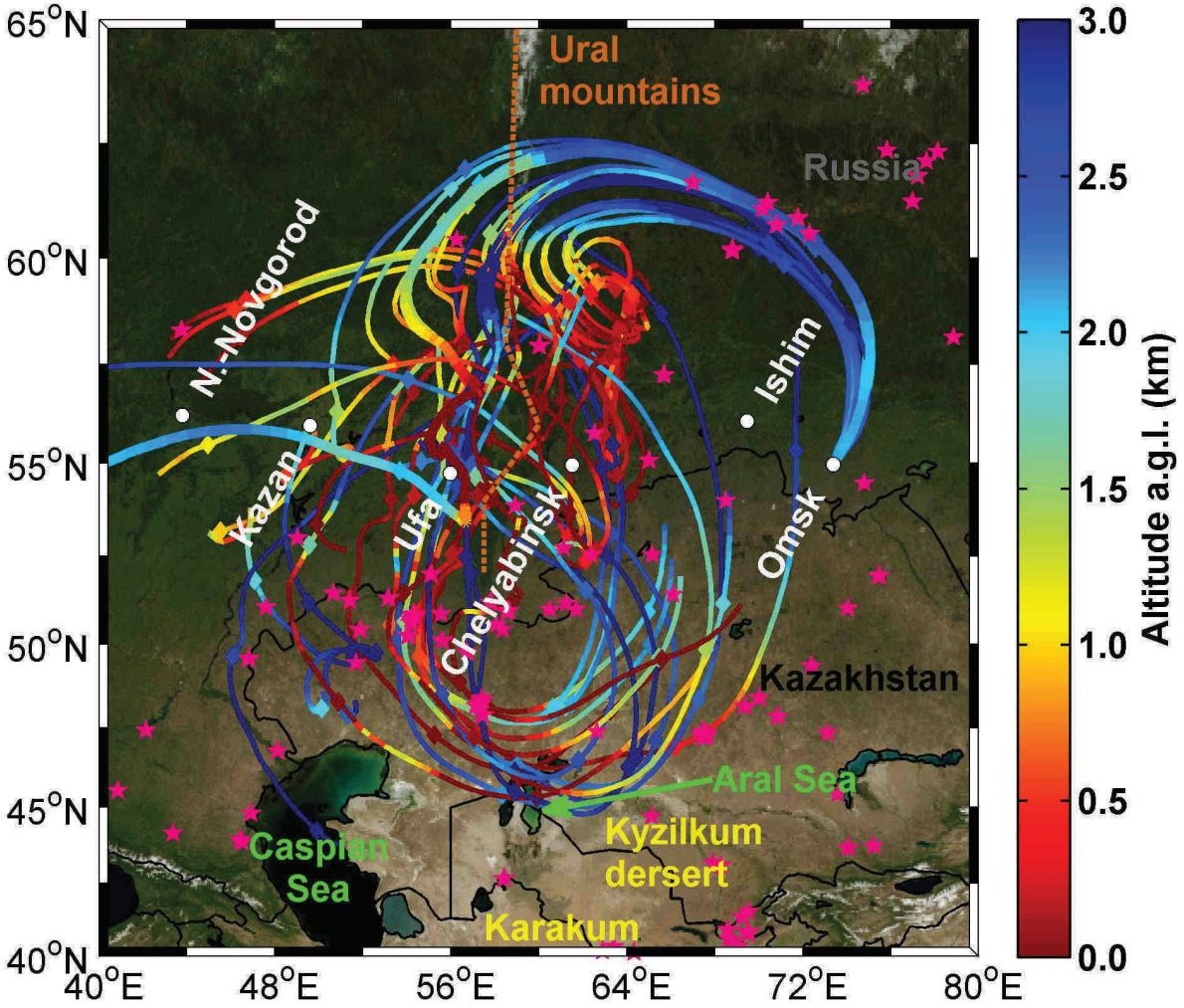

Figure 11. Same as Figure Figure 10, but with trajectories ending in the dust layer observed above Omsk city on June 22nd 2013.

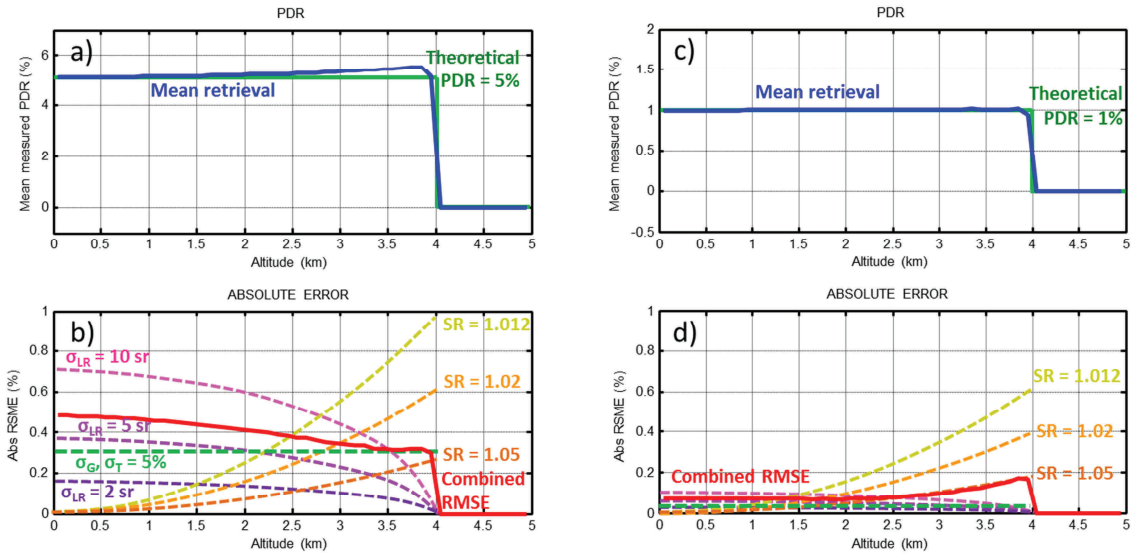

Figure B1. Monte-Carlo simulation of error on PDR measurements in the noise conditions of the Kazan case study; a) mean retrieval for dummy PDR profile of 5% from 0 to 4 km a.gl., b) effects of error parameters and Monte-Carlo simulated Root-Mean-Squared Error for a scattering ratio of 1.05 and an error on LR of 5 sr, c) and d) Same for PDR = 1% from 0 to 4 km.

Signal modelled as Signal(z) = Ks * F(SR(z)) * Rayleigh(z)
Noise modelled as Noise(z) = Kb1*(Signal)^(1/2) + Kb2

Step 1 : calculation of Ks, Kb1 et Kb2 on actual signals

Ex : Nijni – Novgorod to Kazan

On range-corr. signal, est. of Ks (in molecular zone)

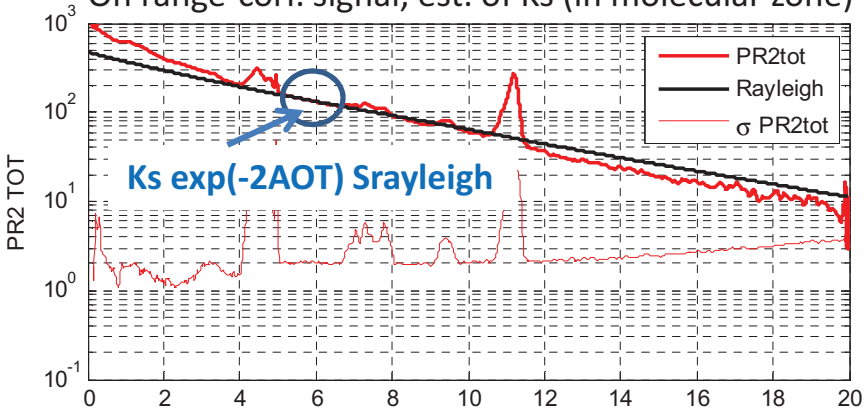

On signal std, est. of Kb (in molecular zone)

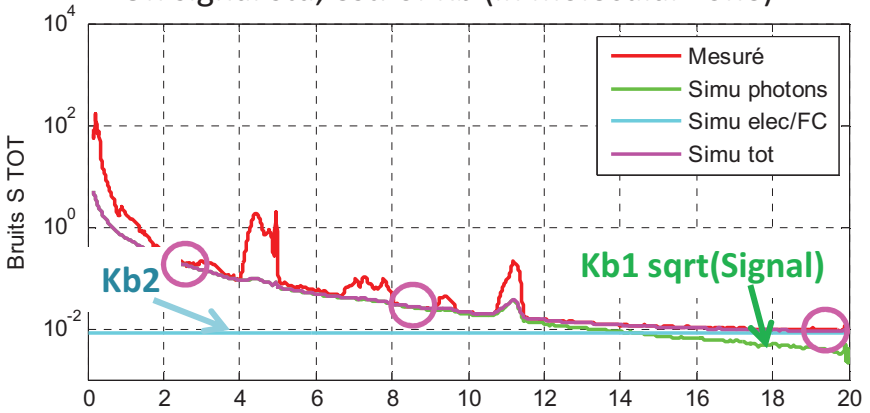

Ks = 5.61E4 exp(2AOT), Kb1 = 2.5E-2, Kb2 = 8E-3

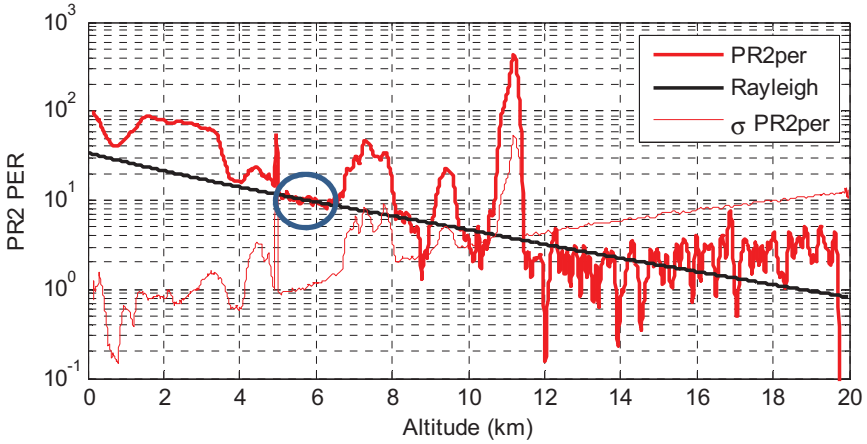

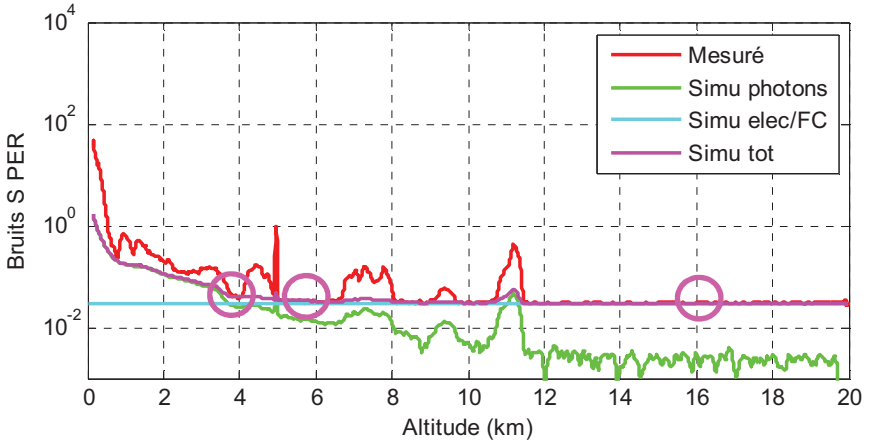

Ks = 4.057E3 exp(2AOT)/0.004, Kb1 = 2.5E-2, Kb2 = 3E-2

Step 2 : signal simulation and processing

Example of dummy signals for PDR = 5%, SR = 1.1, LR = 50
Normalization between 4 and 5 km alt.

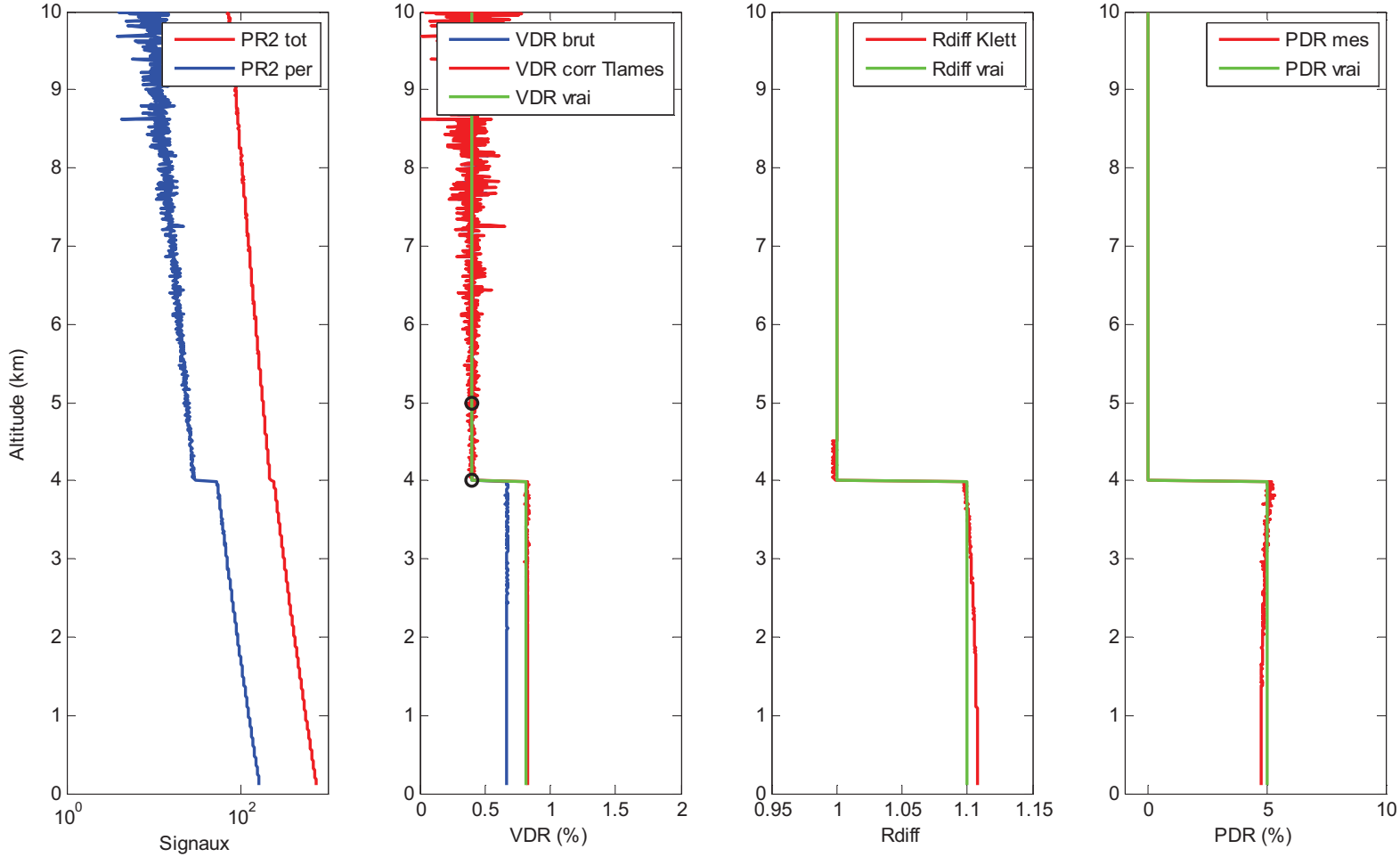

Step 2 : signal simulation and processing

Example of dummy signals for PDR = 5%, SR = 1.1, LR = 50
Noise x4

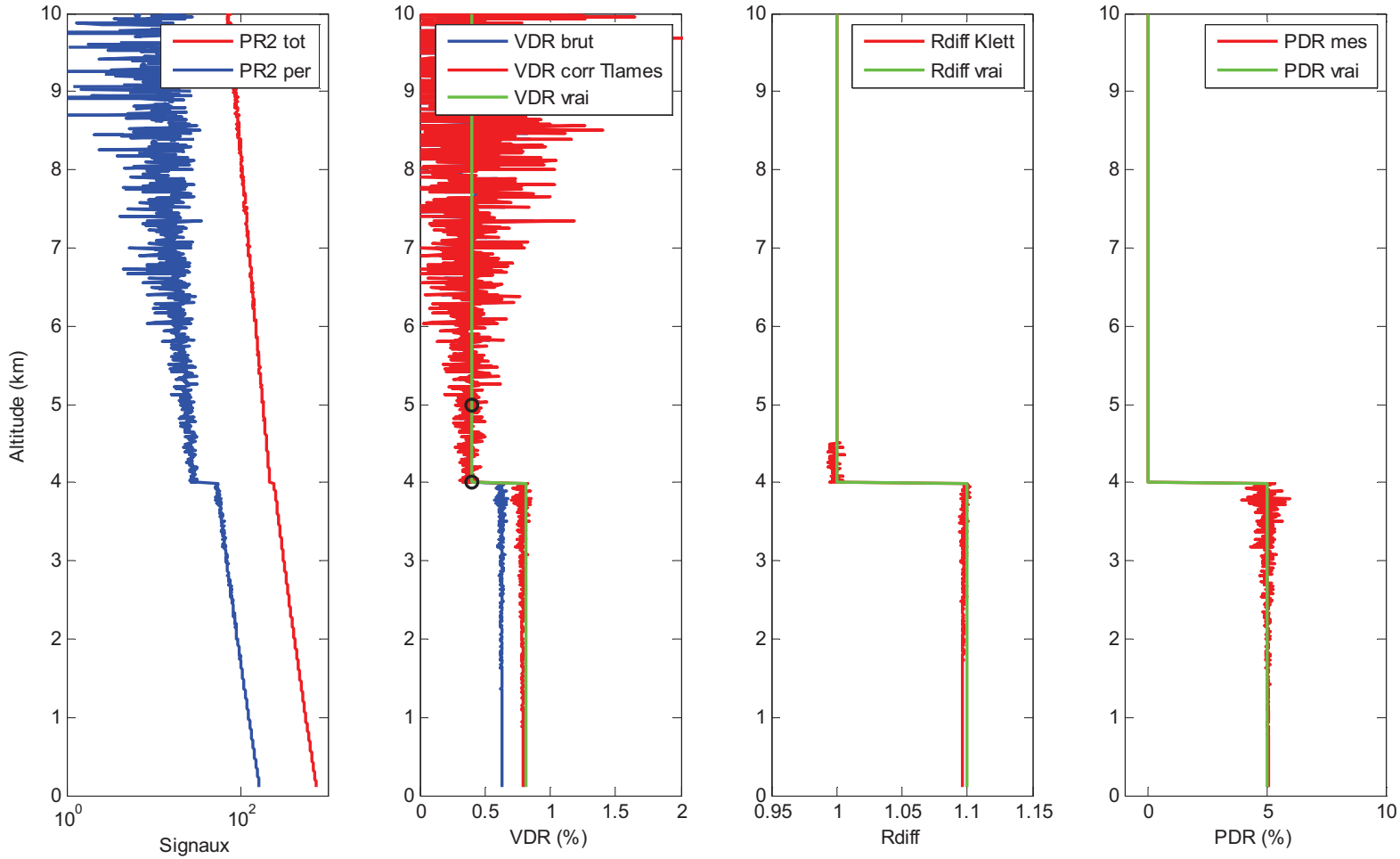

Step 3 : Monte-Carlo simulation of contributions from various noise sources

on the profile of mean measured PDR and RMSE on PDR

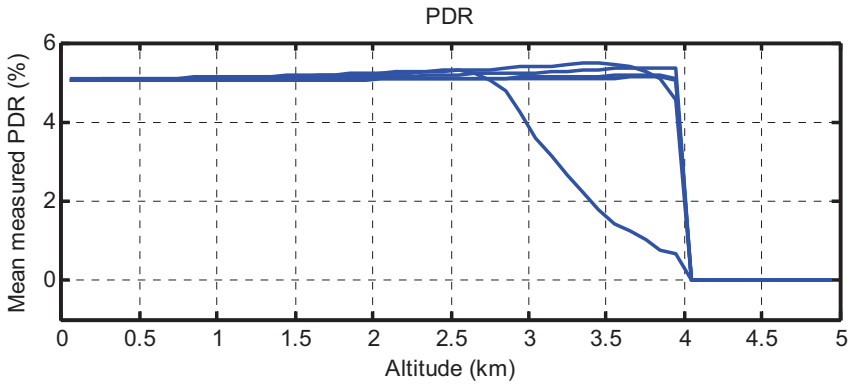

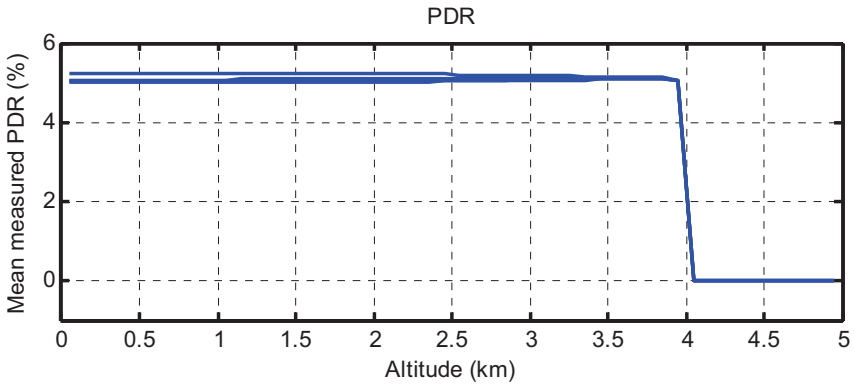

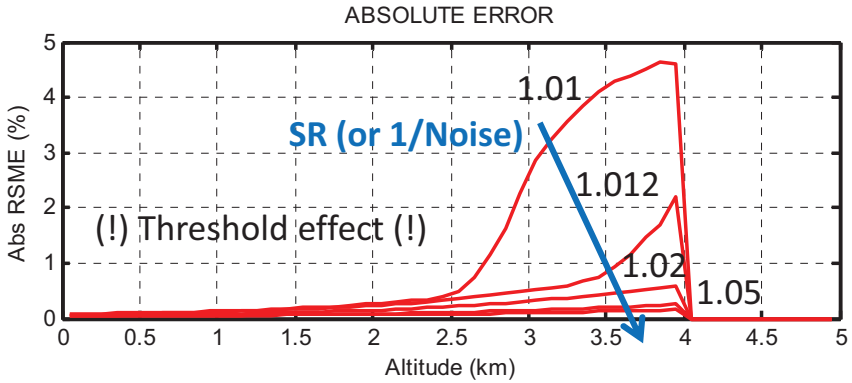

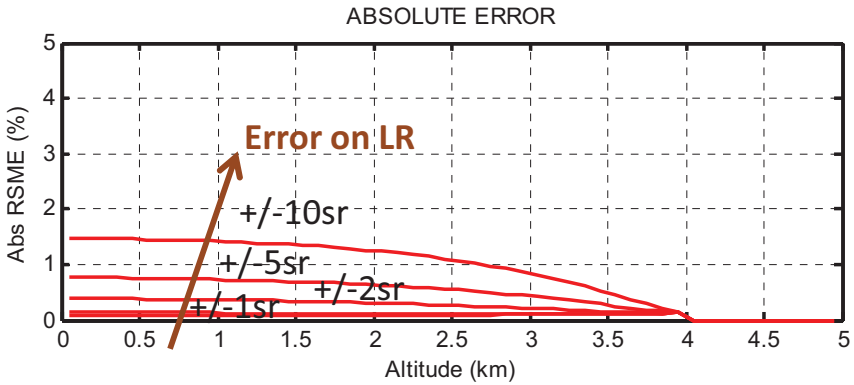

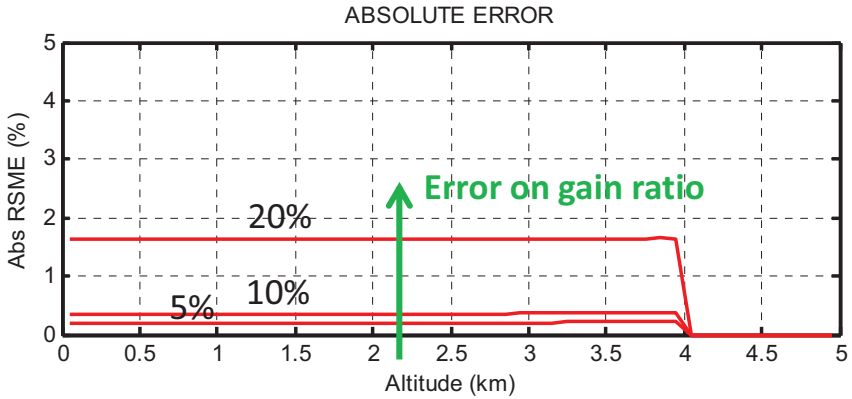

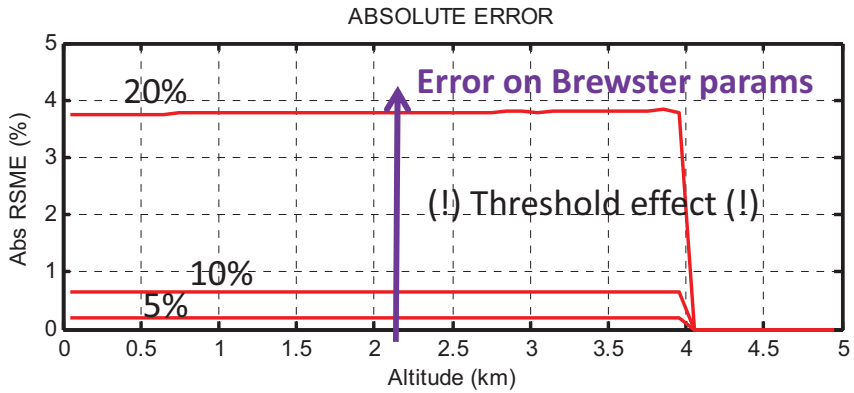

Step 4 : Monte-Carlo simulation under realistic assumptions

PDR = 1% or 5%
SR = 1.01, 1.02 or 1.05

Std(Gain ratio) = 5%
Std(Brewster parameters) = 5%
Std(LR) = 2 sr, 5 sr or 10 sr

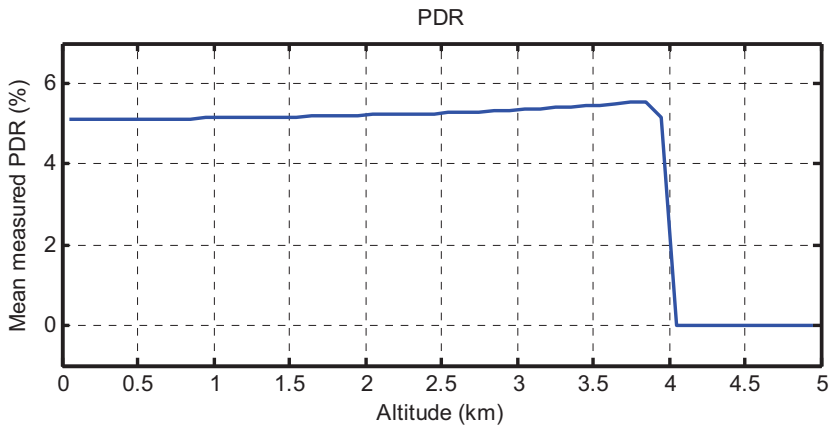

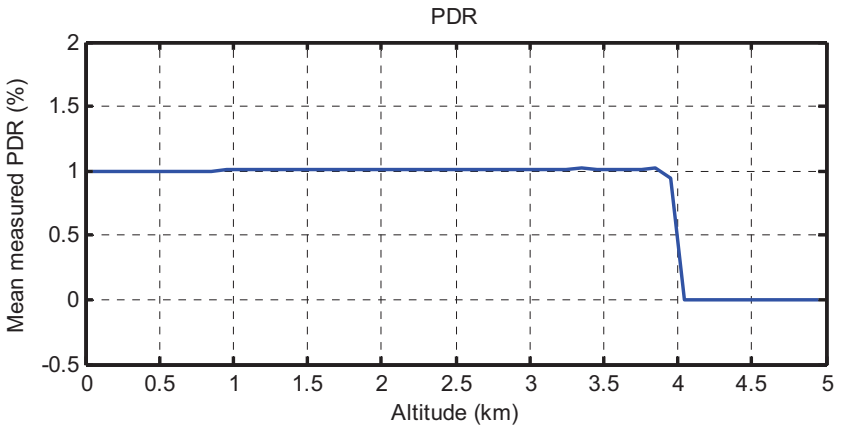

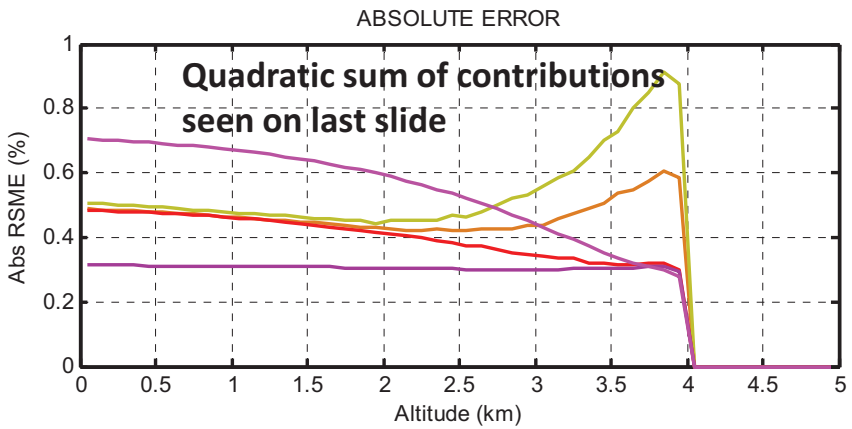

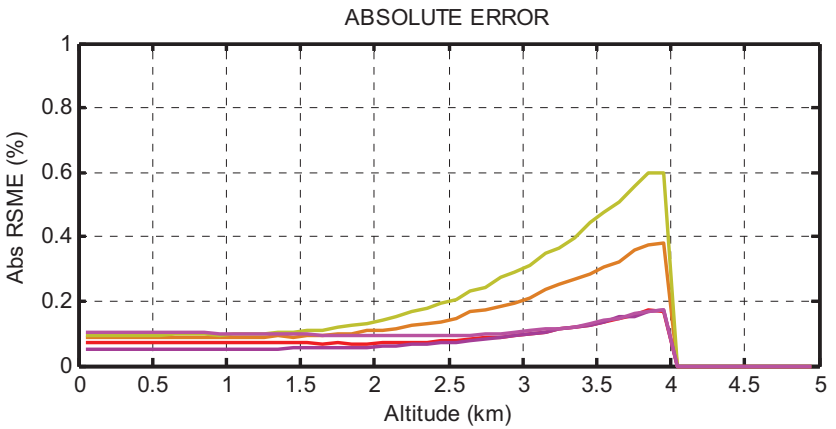

Step 5 : Interpretation and synthesis

Nijni-Kazan case (evening right after dusk)
Worst case scenario for nighttime case study PDR error
Average of 106 profiles (as in case study)
Figure proposed in Appendix B

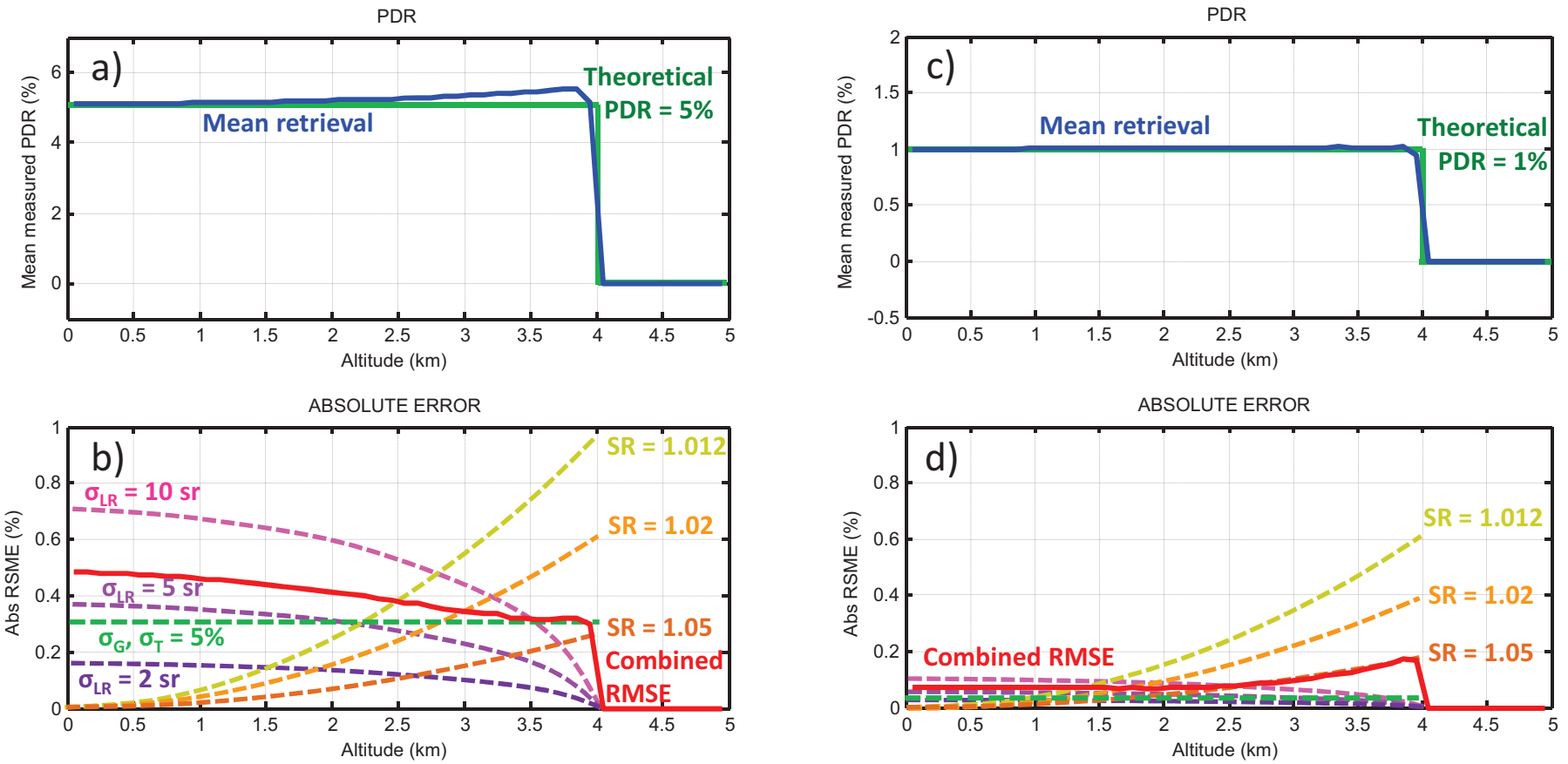

Step 5 : Interpretation and synthesis

Nijni-Kazan case (evening right after dusk)
Worst case scenario for nighttime case study PDR error
Average of 22 profiles only (as in Figures 8 & 9)
60 m (2σ) gaussian vertical smoothing